

Hyperon-nucleon interaction at next-to-leading order in chiral effective field theory

J. Haidenbauer^a, S. Petschauer^b, N. Kaiser^b, U.-G. Meißner^{c,a}, A. Nogga^a, W. Weise^{b,d}

^a*Institute for Advanced Simulation, Institut für Kernphysik and Jülich Center for Hadron Physics, Forschungszentrum Jülich, D-52425 Jülich, Germany*

^b*Physik Department, Technische Universität München, D-85747 Garching, Germany*

^c*Helmholtz Institut für Strahlen- und Kernphysik and Bethe Center for Theoretical Physics, Universität Bonn, D-53115 Bonn, Germany*

^d*ECT*, Villa Tambosi, I-38123 Villazzano (Trento), Italy*

Abstract

Results for the ΛN and ΣN interactions obtained at next-to-leading order in chiral effective field theory are reported. At the order considered there are contributions from one- and two-pseudoscalar-meson exchange diagrams and from four-baryon contact terms without and with two derivatives. $SU(3)$ flavor symmetry is imposed for constructing the hyperon-nucleon interaction while the explicit $SU(3)$ symmetry breaking by the physical masses of the pseudoscalar mesons (π , K , η) is taken into account. An excellent description of the hyperon-nucleon system can be achieved at next-to-leading order. It is on the same level of quality as the one obtained by the most advanced phenomenological hyperon-nucleon interaction models.

Keywords: Hyperon-nucleon interaction, Effective field theory

PACS: 13.75.Ev, 12.39.Fe, 14.20.Pt

1. Introduction

While there is a steady interest in physics involving baryons with strangeness and a corresponding increase of empirical information ever since the discovery of the Λ -hyperon many decades ago, the present times seem to be particularly rewarding. First, at new experimental facilities like J-PARC in Japan or FAIR in Germany a significant amount of beam time will be devoted to strangeness physics research. The proposed experiments encompass accurate measurements of level spectra and decay properties of strangeness $S = -1$ and $S = -2$ hypernuclei [1, 2] but also of elementary cross sections for $\Sigma^+ p$ scattering [3]. Information on Λp scattering, specifically on the scattering lengths, might emerge from ongoing studies of the final-state interaction in production reactions like $pp \rightarrow K^+ \Lambda p$ [4] and $\gamma d \rightarrow K^+ \Lambda n$ [5].

Parallel to this development, techniques for dealing with few- and many-body systems have reached a high degree of sophistication [6, 7, 8, 9, 10, 11, 12, 13]. Some of these allow one to consider nuclei with much more than four nucleons, the limit for standard few-body calculations with the Faddeev-Yakubovsky theory [7]. Of particular interest in this context are nuclear lattice simulations as they offer a new many-body technique directly tailored to the effective field theory description of baryon-baryon interactions, as high-lighted recently by the first ever *ab initio* calculation of the Hoyle state in the spectrum of ^{12}C [14]. Thus, it seems to be feasible to perform similar calculations of hypernuclei too, with comparable accuracy as those for ordinary nuclei, which would open a completely new testing ground for the hyperon-nucleon (YN) interaction. Though few-body calculations of hypernuclei can be already found in the literature [15, 16], for the latter aspect it would be desirable to employ techniques that allow one to use directly the elementary YN interaction (i.e. without any approximation) and, in particular, to include the important Λ - Σ conversion. Only then one can connect the properties of the hypernuclei unambiguously with those of the underlying ΛN (and ΣN) interaction.

Finally, and on a different frontier, lattice QCD calculations have matured to a certain degree, as documented in recent review articles [17, 18], and are coming closer to a level where they can provide additional constraints on the baryon-baryon interactions in the strangeness sector [19].

To keep up with these developments we present here a study of the YN interaction performed at next-to-leading order (NLO) in chiral effective field theory (EFT). It builds upon and extends a previous investigation by the Bonn-Jülich group carried out at leading order (LO) [20]. Using chiral EFT for the YN interaction is prompted by the great success that this scheme has met in the application to the nucleon-nucleon (NN) interaction. Indeed, proposed by Weinberg [21, 22] more than two decades ago, chiral EFT has turned out to be a rather powerful tool for the derivation of nuclear forces. Its most salient feature is that there is an underlying power counting which allows one to improve calculations systematically by going to higher orders in a perturbative expansion. In addition, it is possible to derive two- and three-nucleon forces as well as external current operators in a consistent way. We are now at a stage that the latter aspect will also be important for realistic studies of hypernuclear interactions. In the past there have been already discussions on the role of a three-body YN interaction [23, 24] in hypernuclei and specifically for the properties of neutron star matter [25, 26].

As the most recent applications demonstrate, the nucleon-nucleon interaction can be described accurately within the chiral EFT approach [27, 28]. In line with the original suggestion of Weinberg, the power counting is applied to the NN potential rather than to the reaction amplitude. The latter is obtained from solving a regularized Lippmann-Schwinger equation for the derived interaction potential. The chiral NN potential contains pion-exchanges and a series of contact interactions with an increasing number of derivatives. The latter represent the short-range part of the NN force and are parametrized by low-energy constants (LECs), that need to be fixed by a fit to data. For reviews we refer the reader to the recent Refs. [29, 30].

In our study of the YN interaction, we follow the scheme that has been applied by Epelbaum et al. [28, 31, 32] to the NN interaction. For investigations of the YN interaction based on other schemes see [33, 34]. Still, there are some essential differences between the ΛN , ΣN systems and the NN case that have an influence on how one proceeds in the application of chiral EFT in practice. First and foremost, there is no phase-shift analysis for the $S = -1$ sector and, therefore, we have to fix the LECs by a direct fit to data rather than by a fit to individual partial waves as it is done in the NN case. Secondly, the amount of YN data is rather limited. Indeed, there are basically only integrated cross sections, often with large uncertainties. Thus, we follow here the practice of previous investigations of the YN interaction, notably those performed in the meson-exchange picture [35, 36, 37, 38], and impose constraints from SU(3) flavor symmetry in order to reduce the number of free parameters. In particular, all the baryon-baryon-meson coupling constants are fixed from SU(3) symmetry and the symmetry is also exploited to derive relations between the various LECs. In the actual calculation the SU(3) symmetry is broken, however, by the mass differences between the Goldstone bosons (π , K , η) and between the baryons. For these masses we use the known physical values. In any case, we want to stress that we consider the imposed SU(3) symmetry primarily as a working hypothesis and not as a rigorous constraint. Future data with higher precision will possibly demand to depart from SU(3) symmetry in some way. In that sense our present investigation certainly has primarily an exploratory character. At the moment we are able to describe the available ΛN and ΣN data consistently without any explicit SU(3) breaking in the contact interactions as will be demonstrated below. A simultaneous description of the NN interaction with contact terms that fulfil SU(3) symmetry turned out, however, to be not possible.

As mentioned above, in order to obtain the reaction amplitude from the interaction potential derived within chiral EFT, one has to solve a regularized Lippmann-Schwinger equation. The question how this regularization should be performed is an open issue and is still controversially discussed in the literature, see, e.g. [39, 40, 41, 42]. In the present work, we refrain from touching this certainly very important question. Rather we follow closely the procedure adopted by Epelbaum et al. [28, 32] and others [27], in their study of the NN interaction and introduce a momentum-dependent exponential regulator function into the scattering equation.

The present paper is structured as follows: In Sect. 2, a review of the chiral EFT approach is given with special emphasis on the imposed SU(3) symmetry. In particular, the structure of the contact interactions at LO and NLO is specified and the expression for the one-meson exchange contributions are reproduced. A detailed description of the two-boson exchange potential that arises at NLO is presented in the appendix. The strategy followed in the fit to the data is outlined in Sect. 3. In Sect. 4 results for the ΛN and ΣN interactions obtained at NLO are discussed and compared to available experimental information. Results of our LO calculation and of the Jülich '04 YN interaction [36], a conventional meson-exchange model, are presented, too. The paper ends with a short summary. In the appendix, we provide expressions for the two-boson exchange potential. Furthermore we summarize SU(3) breaking effects which arise at NLO from quark mass insertions in the interaction Lagrangian.

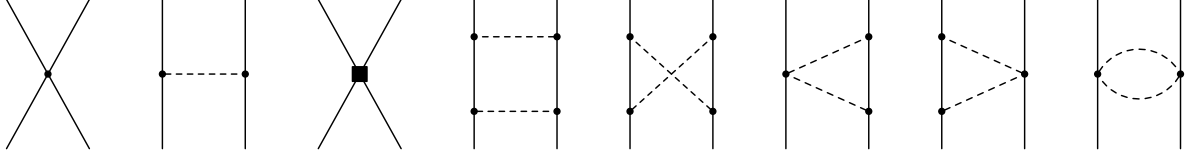


Figure 1: Relevant Feynman diagrams up-to-and-including next-to-leading order. Solid and dashed lines denote octet baryons and pseudoscalar mesons, respectively. The square symbolizes a contact vertex with two derivatives. From left to right: LO contact term, one-meson exchange, NLO contact term, planar box, crossed box, left triangle, right triangle, football diagram.

2. Chiral potential at next-to-leading order

The derivation of the chiral baryon-baryon potentials for the strangeness sector at LO using the Weinberg power counting has been outlined in Refs. [20, 43, 44]. The NLO contributions for the NN case are described in detail in Ref. [32], while the extension to the baryon-baryon case has been worked out in Ref. [45]. The LO potential consists of four-baryon contact terms without derivatives and of one-pseudoscalar-meson exchanges. At NLO contact terms with two derivatives arise, together with loop contributions from (irreducible) two-pseudoscalar-meson exchanges. The corresponding Feynman diagrams are shown in Fig. 1.

2.1. Contact terms

The spin dependence of the potentials due to leading order contact terms is given by [32]

$$V_{BB \rightarrow BB}^{(0)} = C_S + C_T \boldsymbol{\sigma}_1 \cdot \boldsymbol{\sigma}_2, \quad (1)$$

where the parameters C_S and C_T are low-energy constants (LECs) that need to be determined in a fit to data. At next-to-leading order the spin- and momentum-dependence of the contact terms reads

$$\begin{aligned} V_{BB \rightarrow BB}^{(2)} &= C_1 \mathbf{q}^2 + C_2 \mathbf{k}^2 + (C_3 \mathbf{q}^2 + C_4 \mathbf{k}^2) \boldsymbol{\sigma}_1 \cdot \boldsymbol{\sigma}_2 + \frac{i}{2} C_5 (\boldsymbol{\sigma}_1 + \boldsymbol{\sigma}_2) \cdot (\mathbf{q} \times \mathbf{k}) \\ &+ C_6 (\mathbf{q} \cdot \boldsymbol{\sigma}_1) (\mathbf{q} \cdot \boldsymbol{\sigma}_2) + C_7 (\mathbf{k} \cdot \boldsymbol{\sigma}_1) (\mathbf{k} \cdot \boldsymbol{\sigma}_2) + \frac{i}{2} C_8 (\boldsymbol{\sigma}_1 - \boldsymbol{\sigma}_2) \cdot (\mathbf{q} \times \mathbf{k}). \end{aligned} \quad (2)$$

The transferred and average momentum, \mathbf{q} and \mathbf{k} , are defined in terms of the final and initial center-of-mass momenta of the baryons, \mathbf{p}' and \mathbf{p} , as $\mathbf{q} = \mathbf{p}' - \mathbf{p}$ and $\mathbf{k} = (\mathbf{p}' + \mathbf{p})/2$. The C_i ($i = 1, \dots, 8$) are additional LECs depending on the considered baryon-baryon channel. When performing a partial wave projection, these terms contribute to the two S -wave ($^1S_0, ^3S_1$) potentials, the four P -wave ($^1P_1, ^3P_0, ^3P_1, ^3P_2$) potentials, and the 3S_1 - 3D_1 and 1P_1 - 3P_1 transition potentials in the following way [28]:

$$\begin{aligned} V(^1S_0) &= 4\pi(C_S - 3C_T) + \pi(4C_1 + C_2 - 12C_3 - 3C_4 - 4C_6 - C_7)(p^2 + p'^2), \\ &= \tilde{C}_{^1S_0} + C_{^1S_0}(p^2 + p'^2), \end{aligned} \quad (3)$$

$$\begin{aligned} V(^3S_1) &= 4\pi(C_S + C_T) + \frac{\pi}{3}(12C_1 + 3C_2 + 12C_3 + 3C_4 + 4C_6 + C_7)(p^2 + p'^2), \\ &= \tilde{C}_{^3S_1} + C_{^3S_1}(p^2 + p'^2), \end{aligned} \quad (4)$$

$$V(^1P_1) = \frac{2\pi}{3}(-4C_1 + C_2 + 12C_3 - 3C_4 + 4C_6 - C_7) p p' = C_{^1P_1} p p', \quad (5)$$

$$V(^3P_1) = \frac{2\pi}{3}(-4C_1 + C_2 - 4C_3 + C_4 + 2C_5 - 8C_6 + 2C_7) p p' = C_{^3P_1} p p', \quad (6)$$

$$V(^3P_1 - ^1P_1) = -\frac{4\sqrt{2}\pi}{3} C_8 p p' = C_{^3P_1 - ^1P_1} p p', \quad (7)$$

$$V(^1P_1 - ^3P_1) = -\frac{4\sqrt{2}\pi}{3} C_8 p p' = C_{^1P_1-^3P_1} p p', \quad (8)$$

$$V(^3P_0) = \frac{2\pi}{3} (-4C_1 + C_2 - 4C_3 + C_4 + 4C_5 + 12C_6 - 3C_7) p p' = C_{^3P_0} p p', \quad (9)$$

$$V(^3P_2) = \frac{2\pi}{3} (-4C_1 + C_2 - 4C_3 + C_4 - 2C_5) p p' = C_{^3P_2} p p', \quad (10)$$

$$V(^3D_1 - ^3S_1) = \frac{2\sqrt{2}\pi}{3} (4C_6 + C_7) p'^2 = C_{^3S_1-^3D_1} p'^2, \quad (11)$$

$$V(^3S_1 - ^3D_1) = \frac{2\sqrt{2}\pi}{3} (4C_6 + C_7) p^2 = C_{^3S_1-^3D_1} p^2, \quad (12)$$

with $p = |\mathbf{p}|$ and $p' = |\mathbf{p}'|$. Note that the term proportional to C_8 in Eqs. (7) and (7) represents an antisymmetric spin-orbit force and gives rise to spin singlet-triplet transitions (i.e. $^1P_1 - ^3P_1$). Such transitions cannot occur in the NN interaction, unless isospin symmetry breaking is included, and, therefore, this term is absent in the equations given in Ref. [32]. However, in general, this antisymmetric spin-orbit term is allowed. Specifically, it does not break SU(3) symmetry.

Assuming only isospin symmetry, the LECs for each spin-isospin channel of the various $BB \rightarrow BB$ interaction potentials are independent. When imposing SU(3) flavor symmetry one obtains relations between the LECs and, thereby, the number of terms that need to be fitted to data gets reduced. The relevant SU(3) structure for the scattering of two octet baryons follows from the tensor product decomposition $8 \otimes 8 = 1 \oplus 8_a \oplus 8_s \oplus 10^* \oplus 10 \oplus 27$ (for details see Refs. [46, 47]). With that one can express all the $C_{^1S_0, \nu}, C_{^3S_1, \nu}, \dots$, in Eqs. (3) – (12) ($\nu = NN \rightarrow NN, \Lambda N \rightarrow \Lambda N, \Lambda N \rightarrow \Sigma N, \Sigma N \rightarrow \Sigma N$) by coefficients corresponding to the SU(3) irreducible representations: $C^1, C^{8_a}, C^{8_s}, C^{10^*}, C^{10}, C^{27}$. The particular combinations of LECs in the various $BB \rightarrow BB$ channels and for the various partial waves are summarized in Tab. 1. For example, for the potential in the 1S_0 partial wave of the $\Lambda N \rightarrow \Lambda N$ channel we get

$$V_{\Lambda N \rightarrow \Lambda N}(^1S_0) = \frac{1}{10} \left[9\tilde{C}_{^1S_0}^{27} + \tilde{C}_{^1S_0}^{8_s} + (9C_{^1S_0}^{27} + C_{^1S_0}^{8_s})(p^2 + p'^2) \right]. \quad (13)$$

Note that Tab. 1 gives the weight factors of the various baryon-baryon channels with respect to the irreducible SU(3) representations. In addition, it reflects the constraints from the generalized Pauli principle. The interaction in partial waves like the $^3S_1, ^3D_1$, and 1P_1 , which are symmetric with regard to their spin-space component, is given by linear combinations of coefficients corresponding to antisymmetric SU(3) representations ($C^{8_a}, C^{10^*}, C^{10}$), whereas those with antisymmetric spin-space part ($^1S_0, ^3P_0, ^3P_1, ^3P_2$) receive only contributions from symmetric representations (C^{8_s}, C^{27}). The C_8 -term induces transitions between singlet and triplet states in the octet-representation 8_a and 8_s , respectively [47]. For a detailed derivation of the SU(3) constraints on the LECs see Ref. [20] or [48].

Due to the imposed SU(3) constraints at LO there are only five independent LECs for the NN and the YN sectors together, as outlined in Ref. [20]. Note that without SU(3) symmetry, there would be twice as many. At NLO SU(3) symmetry implies that in case of the NN and YN interactions there are eight new LECs entering the S -waves and S - D transitions, respectively, and ten coefficients in the P -waves. Note that the sixth leading-order LEC corresponding to the singlet representation (C^1) is present in the strangeness $S = -2$ channels with isospin $I = 0$ [49] and there are four more LECs that contribute to the $S = -2$ sector at NLO.

2.2. Goldstone boson exchange

The one- and two-pseudoscalar-meson-exchange potentials follow from the SU(3)-invariant meson-baryon interaction Lagrangian

$$\mathcal{L}_{\text{MB}} = \text{tr} \left(\bar{B} (i\gamma^\mu D_\mu - M_0) B \right) - \frac{D}{2} \text{tr} \left(\bar{B} \gamma^\mu \gamma_5 \{u_\mu, B\} \right) - \frac{F}{2} \text{tr} \left(\bar{B} \gamma^\mu \gamma_5 [u_\mu, B] \right), \quad (14)$$

with $D_\mu B = \partial_\mu B + [\Gamma_\mu, B]$, $\Gamma_\mu = \frac{1}{2}(u^\dagger \partial_\mu u + u \partial_\mu u^\dagger)$ and $u_\mu = i(u^\dagger \partial_\mu u - u \partial_\mu u^\dagger)$, and where the trace is taken in flavor space. The constant M_0 denotes the baryon mass in the three-flavor chiral limit. The coupling constants F and D satisfy the relation $F + D = g_A \simeq 1.26$, where g_A is the axial-vector strength measured in neutron β -decay. For the

Table 1: SU(3) relations for the various contact potentials in the isospin basis. C_ξ^{27} etc. refers to the corresponding irreducible SU(3) representation for a particular partial wave ξ . The actual potential still needs to be multiplied by pertinent powers of the momenta p and p' .

	Channel	I	$V(\xi)$		
			$\xi = {}^1S_0, {}^3P_0, {}^3P_1, {}^3P_2$	$\xi = {}^3S_1, {}^3S_1-{}^3D_1, {}^1P_1$	$\xi = {}^1P_1-{}^3P_1$
$S = 0$	$NN \rightarrow NN$	0	–	$C_\xi^{10^*}$	–
	$NN \rightarrow NN$	1	C_ξ^{27}	–	–
$S = -1$	$\Lambda N \rightarrow \Lambda N$	$\frac{1}{2}$	$\frac{1}{10}(9C_\xi^{27} + C_\xi^{8_s})$	$\frac{1}{2}(C_\xi^{8_a} + C_\xi^{10^*})$	$\frac{-1}{\sqrt{20}}C_\xi^{8_s, 8_a}$
	$\Lambda N \rightarrow \Sigma N$	$\frac{1}{2}$	$\frac{3}{10}(-C_\xi^{27} + C_\xi^{8_s})$	$\frac{1}{2}(-C_\xi^{8_a} + C_\xi^{10^*})$	$\frac{3}{\sqrt{20}}C_\xi^{8_s, 8_a}$
	$\Sigma N \rightarrow \Lambda N$	$\frac{1}{2}$	$\frac{1}{10}(C_\xi^{27} + 9C_\xi^{8_s})$	$\frac{1}{2}(C_\xi^{8_a} + C_\xi^{10^*})$	$\frac{-1}{\sqrt{20}}C_\xi^{8_s, 8_a}$
	$\Sigma N \rightarrow \Sigma N$	$\frac{1}{2}$	$\frac{1}{10}(C_\xi^{27} + 9C_\xi^{8_s})$	$\frac{1}{2}(C_\xi^{8_a} + C_\xi^{10^*})$	$\frac{3}{\sqrt{20}}C_\xi^{8_s, 8_a}$
	$\Sigma N \rightarrow \Sigma N$	$\frac{3}{2}$	C_ξ^{27}	C_ξ^{10}	–

pseudoscalar mesons and octet baryons, collected in traceless 3×3 matrices,

$$P = \begin{pmatrix} \frac{\pi^0}{\sqrt{2}} + \frac{\eta}{\sqrt{6}} & \pi^+ & K^+ \\ \pi^- & -\frac{\pi^0}{\sqrt{2}} + \frac{\eta}{\sqrt{6}} & K^0 \\ K^- & \bar{K}^0 & -\frac{2\eta}{\sqrt{6}} \end{pmatrix}, \quad B = \begin{pmatrix} \frac{\Sigma^0}{\sqrt{2}} + \frac{\Lambda}{\sqrt{6}} & \Sigma^+ & p \\ \Sigma^- & -\frac{\Sigma^0}{\sqrt{2}} + \frac{\Lambda}{\sqrt{6}} & n \\ -\Xi^- & \Xi^0 & -\frac{2\Lambda}{\sqrt{6}} \end{pmatrix}, \quad (15)$$

we use the usual non-linear realization of chiral symmetry with $U(x) = u^2(x) = \exp(i\sqrt{2}P(x)/f_0)$, and f_0 is the Goldstone boson decay constant in the chiral limit. These fields transform under the chiral group $SU(3)_L \times SU(3)_R$ as $U \rightarrow RUL^\dagger$ and $B \rightarrow KBK^\dagger$ with $L \in SU(3)_L, R \in SU(3)_R$ and the SU(3) valued compensator field $K = K(L, R, U)$, cf. Ref. [50]. After an expansion of the interaction Lagrangian in powers of P one obtains from the terms proportional to D and F the pseudovector coupling term

$$\mathcal{L}_1 = -\frac{\sqrt{2}}{2f_0} \text{tr} \left(D \bar{B} \gamma^\mu \gamma_5 \left\{ \partial_\mu P, B \right\} + F \bar{B} \gamma^\mu \gamma_5 \left[\partial_\mu P, B \right] \right), \quad (16)$$

which leads to a vertex between two baryons and one meson. In the same way, the term involving the chiral connection Γ_μ gives

$$\mathcal{L}_2 = \frac{1}{4f_0^2} \text{tr} \left(i \bar{B} \gamma^\mu \left[[P, \partial_\mu P], B \right] \right), \quad (17)$$

which describes a (Weinberg-Tomozawa) vertex between two baryons and two mesons.

When writing the pseudovector interaction Lagrangian \mathcal{L}_1 explicitly in the isospin basis, one gets

$$\begin{aligned} \mathcal{L}_1 = & -f_{NN\pi} \bar{N} \gamma^\mu \gamma_5 \tau N \cdot \partial_\mu \pi + i f_{\Sigma\Sigma\pi} \bar{\Sigma} \gamma^\mu \gamma_5 \times \Sigma \cdot \partial_\mu \pi \\ & - f_{\Lambda\Sigma\pi} \left[\bar{\Lambda} \gamma^\mu \gamma_5 \Sigma + \bar{\Sigma} \gamma^\mu \gamma_5 \Lambda \right] \cdot \partial_\mu \pi - f_{\Xi\Xi\pi} \bar{\Xi} \gamma^\mu \gamma_5 \tau \Xi \cdot \partial_\mu \pi \\ & - f_{\Lambda NK} \left[\bar{N} \gamma^\mu \gamma_5 \Lambda \partial_\mu K + \text{h.c.} \right] - f_{\Xi \Lambda K} \left[\bar{\Xi} \gamma^\mu \gamma_5 \Lambda \partial_\mu \bar{K} + \text{h.c.} \right] \\ & - f_{\Sigma NK} \left[\bar{N} \gamma^\mu \gamma_5 \tau \partial_\mu K \cdot \Sigma + \text{h.c.} \right] - f_{\Sigma \Xi K} \left[\bar{\Xi} \gamma^\mu \gamma_5 \tau \partial_\mu \bar{K} \cdot \Sigma + \text{h.c.} \right] \\ & - f_{NN\eta_8} \bar{N} \gamma^\mu \gamma_5 N \partial_\mu \eta - f_{\Lambda\Lambda\eta_8} \bar{\Lambda} \gamma^\mu \gamma_5 \Lambda \partial_\mu \eta \\ & - f_{\Sigma\Sigma\eta_8} \bar{\Sigma} \cdot \gamma^\mu \gamma_5 \Sigma \partial_\mu \eta - f_{\Xi\Xi\eta_8} \bar{\Xi} \gamma^\mu \gamma_5 \Xi \partial_\mu \eta. \end{aligned} \quad (18)$$

Here, we have introduced the isospin doublets

$$N = \begin{pmatrix} p \\ n \end{pmatrix}, \quad \Xi = \begin{pmatrix} \Xi^0 \\ \Xi^- \end{pmatrix}, \quad K = \begin{pmatrix} K^+ \\ K^0 \end{pmatrix}, \quad \bar{K} = \begin{pmatrix} \bar{K}^0 \\ -K^- \end{pmatrix}. \quad (19)$$

Table 2: Isospin factors \mathcal{I} for the various one-pseudoscalar-meson exchanges.

	Channel	Isospin	π	K	η
$S = 0$	$NN \rightarrow NN$	0	-3	0	1
		1	1	0	1
$S = -1$	$\Lambda N \rightarrow \Lambda N$	$\frac{1}{2}$	0	1	1
	$\Lambda N \rightarrow \Sigma N$	$\frac{1}{2}$	$-\sqrt{3}$	$-\sqrt{3}$	0
	$\Sigma N \rightarrow \Sigma N$	$\frac{1}{2}$	-2	-1	1
		$\frac{3}{2}$	1	2	1

The signs have been chosen according to the conventions of Ref. [46], such that the inner product of the isovector Σ (or π) defined in spherical components reads

$$\Sigma \cdot \Sigma = \sum_m (-1)^m \Sigma_m \Sigma_{-m} = \Sigma^+ \Sigma^- + \Sigma^0 \Sigma^0 + \Sigma^- \Sigma^+ . \quad (20)$$

Since the original interaction Lagrangian in Eq. (16) is SU(3)-invariant, the various coupling constants are related to each other by [46]

$$\begin{aligned} f_{NN\pi} &= f, & f_{NN\eta_8} &= \frac{1}{\sqrt{3}}(4\alpha - 1)f, & f_{\Lambda NK} &= -\frac{1}{\sqrt{3}}(1 + 2\alpha)f, \\ f_{\Xi\Xi\pi} &= -(1 - 2\alpha)f, & f_{\Xi\Xi\eta_8} &= -\frac{1}{\sqrt{3}}(1 + 2\alpha)f, & f_{\Xi\Lambda K} &= \frac{1}{\sqrt{3}}(4\alpha - 1)f, \\ f_{\Lambda\Sigma\pi} &= \frac{2}{\sqrt{3}}(1 - \alpha)f, & f_{\Sigma\Sigma\eta_8} &= \frac{2}{\sqrt{3}}(1 - \alpha)f, & f_{\Sigma NK} &= (1 - 2\alpha)f, \\ f_{\Sigma\Sigma\pi} &= 2\alpha f, & f_{\Lambda\Lambda\eta_8} &= -\frac{2}{\sqrt{3}}(1 - \alpha)f, & f_{\Xi\Sigma K} &= -f. \end{aligned} \quad (21)$$

Evidently, all coupling constants are given in terms of $f \equiv g_A/2f_0$ and the ratio $\alpha = F/(F + D)$.

The expression for the one-pseudoscalar-meson exchange potential is similar to the standard one-pion-exchange potential [32]

$$V_{B_1 B_2 \rightarrow B_3 B_4}^{OBE} = -f_{B_1 B_3 P} f_{B_2 B_4 P} \frac{(\boldsymbol{\sigma}_1 \cdot \mathbf{q})(\boldsymbol{\sigma}_2 \cdot \mathbf{q})}{\mathbf{q}^2 + m_P^2} \mathcal{I}_{B_1 B_2 \rightarrow B_3 B_4} . \quad (22)$$

Here, m_P is the mass of the exchanged pseudoscalar meson. In the present calculation we use the physical masses m_π, m_K, m_η in Eq. (22). Thus, the explicit SU(3) breaking reflected in the mass splitting between the pseudoscalar mesons is taken into account. The η meson is identified with the octet-state η_8 . The isospin factors $\mathcal{I}_{B_1 B_2 \rightarrow B_3 B_4}$ are given in Tab. 2.

The two-pseudoscalar-meson exchange potential, built up by a set of one-loop diagrams, is described in detail in Appendix A. Relativistic corrections to the one-meson exchange potential that arise at NLO due to differences of the baryon masses are discussed in Appendix B.

2.3. Scattering equation

In the actual calculation a partial-wave projection of the interaction potentials is performed, as described in detail in Ref. [20]. The reaction amplitudes are obtained from the solution of a coupled-channel Lippmann-Schwinger (LS) equation:

$$T_{\nu\nu'}^{\rho\rho',J}(p'', p'; \sqrt{s}) = V_{\nu\nu'}^{\rho\rho',J}(p'', p') + \sum_{\rho,\nu} \int_0^\infty \frac{dp p^2}{(2\pi)^3} V_{\nu''\nu'''}^{\rho''\rho'',J}(p'', p) \frac{2\mu_\nu}{q_\nu^2 - p^2 + i\eta} T_{\nu\nu'}^{\rho\rho',J}(p, p'; \sqrt{s}) . \quad (23)$$

Here, the label ν indicates the particle channels and the label ρ the partial wave. μ_ν is the pertinent reduced baryon mass. The on-shell momentum q_ν in the intermediate state, is determined by $\sqrt{s} = \sqrt{M_{B_{1,\nu}}^2 + q_\nu^2} + \sqrt{M_{B_{2,\nu}}^2 + q_\nu^2}$. Relativistic kinematics is used for relating the laboratory momentum p_{lab} of the hyperons to the center-of-mass momentum.

We solve the LS equation in the particle basis, in order to incorporate the correct physical thresholds. Depending on the total charge, up to three baryon-baryon channels can couple. The Coulomb interaction is taken into account appropriately via the Vincent-Phatak method [51]. The potentials in the LS equation are cut off with a regulator function, $f_R(\Lambda) = \exp[-(p^4 + p^4)/\Lambda^4]$, in order to remove high-energy components [28]. We consider cutoff values in the range $\Lambda = 450 - 700$ MeV, similar to what was used for chiral NN potentials [28], but anticipate here already that the best results are achieved for cutoffs located in the interval 500 – 650 MeV.

3. Fitting procedure

For the fitting procedure we consider the same “standard” set of 36 YN data points that have been used in our previous works [20, 36] as also done by the Nijmegen group in their investigations [37]. This data set consists of low-energy total cross sections for the reactions: $\Lambda p \rightarrow \Lambda p$ from Ref. [52] (6 data points) and Ref. [53] (6 data points), $\Sigma^- p \rightarrow \Lambda n$ [54] (6 data points), $\Sigma^- p \rightarrow \Sigma^0 n$ [54] (6 data points), $\Sigma^- p \rightarrow \Sigma^- p$ [55] (7 data points), $\Sigma^+ p \rightarrow \Sigma^+ p$ [55] (4 data points), and the inelastic capture ratio at rest [56, 57]. Besides these YN data the empirical binding energy of the hypertriton ${}^3_\Lambda\text{H}$ is used as a further constraint. Otherwise it would not be possible to fix the relative strength of the spin-singlet and spin-triplet S -wave contributions to the Λp interaction.

We recall that there are in total five independent LECs at LO, that describe the NN and YN interactions, see Tab. 1. In Ref. [20] a fit to the YN scattering data at LO was presented utilizing these five contact terms. It turned out that already in that scenario a fairly reasonable description of the 36 low-energy YN scattering data could be achieved for cutoffs $\Lambda = 550 - 700$ MeV and for natural values of the LECs. At NLO there are eight new contact terms contributing to the S -waves and the ${}^3S_1 - {}^3D_1$ transition, and ten in the P -waves. As described in Sect. 2.1, we impose SU(3) flavor symmetry in order to reduce the number of LECs that need to be determined. Without implementing this constraint there would be 20 independent contact terms for the ΛN and ΣN systems in the S -waves (and the S - D transitions) alone, and, given the low number of data points together with their large error bars, it is simply impossible to fix all those LECs by a fit to the available empirical information.

In the actual fitting procedure, first, we have considered only the 13 LECs in the S -waves and the S - D transitions. After all, the available YN data consist practically only of total cross sections at low energies and these are predominantly determined by the S -wave amplitudes. The fits are performed for fixed values of the cutoff scale where we started with $\Lambda = 600$ MeV. The subsequent fits for other cutoffs were done under the constraint that the results should stay as close as possible to those obtained with $\Lambda = 600$ MeV, for the singlet and triplet cross sections separately. This procedure is demanded by our requirement to reproduce the hypertriton as mentioned above.

Note that for the $\Sigma^+ p \rightarrow \Sigma^+ p$ and $\Sigma^- p \rightarrow \Sigma^- p$ channels the experimental total cross sections were obtained by incomplete angular coverage [55]:

$$\sigma = \frac{2}{\cos \theta_{\max} - \cos \theta_{\min}} \int_{\cos \theta_{\min}}^{\cos \theta_{\max}} \frac{d\sigma(\theta)}{d \cos \theta} d \cos \theta. \quad (24)$$

Following Ref. [37], we use $\cos \theta_{\min} = -0.5$ and $\cos \theta_{\max} = 0.5$ in our calculations for the $\Sigma^+ p \rightarrow \Sigma^+ p$ and $\Sigma^- p \rightarrow \Sigma^- p$ cross sections, in order to stay as close as possible to the experimental procedure. The total cross sections for the other channels are evaluated by simply integrating the differential cross sections over the whole angular region.

For the capture ratio at rest, r_R , we follow the definition of Ref. [58]:

$$r_R = \frac{1}{4} \frac{\sigma_s(\Sigma^- p \rightarrow \Sigma^0 n)}{\sigma_s(\Sigma^- p \rightarrow \Lambda n) + \sigma_s(\Sigma^- p \rightarrow \Sigma^0 n)} + \frac{3}{4} \frac{\sigma_t(\Sigma^- p \rightarrow \Sigma^0 n)}{\sigma_t(\Sigma^- p \rightarrow \Lambda n) + \sigma_t(\Sigma^- p \rightarrow \Sigma^0 n)}, \quad (25)$$

where σ_s is the total reaction cross section in the singlet 1S_0 partial wave, and σ_t the total reaction cross section in the triplet-coupled ${}^3S_1 - {}^3D_1$ partial waves. The cross sections are the ones at zero momentum, but following common practice [37] we evaluate the cross sections at a small non-zero momentum, namely $p_{\text{lab}} = 10$ MeV/ c .

While the χ^2 fit to the 36 data points allowed us to fix the majority of the S -wave LECs it turned out that concerning the 3S_1 partial wave in the $I = 3/2$ ΣN channel, solutions with either a positive (attractive) or a negative (repulsive) phase shift are possible. This can be understood from the SU(3) structure as given in Table 1 which shows that this partial wave is controlled by the “isolated” 10 representation such that the corresponding LECs do not enter in any

Table 3: The YN contact terms for the 1S_0 and 3S_1 - 3D_1 partial waves for various cut-offs. The values of the \tilde{C} 's are in 10^4 GeV^{-2} the ones of the C 's in 10^4 GeV^{-4} ; the values of Λ in MeV.

Λ		450	500	550	600	650	700
1S_0	$\tilde{C}_{^1S_0}^{27}$	-0.0893	-0.0672	0.00648	0.1876	0.6140	1.145
	$\tilde{C}_{^1S_0}^{8_s}$	0.2000	0.1970	0.1930	0.1742	0.1670	0.1730
	$C_{^1S_0}^{27}$	1.500	1.800	2.010	2.200	2.400	2.410
	$C_{^1S_0}^{8_s}$	-0.200	-0.200	-0.206	-0.0816	-0.0597	0.1000
3S_1 - 3D_1	$\tilde{C}_{^3S_1}^{10}$	0.104	0.541	0.149	0.344	0.499	0.560
	$\tilde{C}_{^3S_1}^{10^*}$	0.171	0.209	0.635	1.420	2.200	2.960
	$\tilde{C}_{^3S_1}^{8_a}$	0.0218	0.00715	-0.0143	-0.0276	-0.0269	0.00173
	$C_{^3S_1}^{10}$	2.240	2.310	2.450	2.740	2.530	2.030
	$C_{^3S_1}^{10^*}$	0.310	0.143	0.741	1.090	1.150	1.120
	$C_{^3S_1}^{8_a}$	0.373	0.469	0.627	0.775	0.854	0.964
	$C_{^3S_1-^3D_1}^{10}$	-0.360	-0.429	-0.428	-0.191	-0.191	-0.122
	$C_{^3S_1-^3D_1}^{10^*}$	-0.300	-0.300	-0.356	-0.380	-0.380	-0.228
	$C_{^3S_1-^3D_1}^{8_a}$	0.0356	0.0475	0.0453	-0.00621	-0.00621	-0.0497

of the other YN channels. We adopt here the repulsive solution in accordance with evidence from recently measured (π^- , K^+) inclusive spectra related to Σ^- -formation in heavy nuclei [59, 60, 61], which suggest a repulsive Σ -nucleus single-particle potential [62, 63].

We should also mention that we observe some correlations between the values of the S -wave LECs at LO and NLO, i.e. \tilde{C} and C in Eqs. (3) and (4). This is a consequence of the fact that the fitted ΣN cross sections lie all within a rather narrow energy interval near threshold so that there is only a fairly weak sensitivity to the momentum-dependent ($p^2 + p'^2$) terms. The Λp cross sections alone, which are known over a larger energy range, are not sufficient for separating the strength of \tilde{C} and C .

The limited number (and quality) of differential cross sections and the complete lack of polarization observables makes a determination of the contact terms in the P -waves from YN data practically impossible. Therefore, in this case and in line with the power counting we assume strict SU(3) symmetry for the contact terms and use the NN P -wave phase shifts as a further constraint. In particular, we fix the LECs C^{27} and C^{10^*} from fitting to empirical 1P_1 , 3P_0 , and 3P_1 NN -phase shifts [64] in the region of $25 \leq T_{\text{lab}} \leq 50$ MeV [32]. The 3P_2 partial wave is special. Here a NLO calculation with the pertinent LEC determined from the low-energy region yields results at higher energies that strongly overestimate the empirical phase shifts, see, e.g. Ref. [28]. Such a LEC would likewise lead to a considerable overestimation of the Λp cross section around and above the ΣN threshold. In order to avoid this we fix this specific LEC from the NN -phase shifts in an energy region corresponding to the ΣN threshold, namely $T_{\text{lab}} \approx 150$ MeV.

Utilizing the NN -phase shifts reduces the number of P -wave contact terms that need to be determined in the YN sector by roughly a factor two. Here the most important constraint is provided by the Λp cross section above the ΣN threshold, i.e. at around $p_{\text{lab}} \approx 800$ MeV/c, which is roughly 10 mb according to experiments [65, 66]. Agreement with these data can be only achieved if the contributions from each of the P -waves (1P_1 , 3P_0 , 3P_1 , 3P_2) is kept small, which means in turn that the corresponding phase shifts have to be small. The differential cross section for $\Sigma^- p \rightarrow \Lambda n$ has been measured at two energies near the ΣN threshold and it is sensitive to the P -waves, too. We used this empirical information to fix the remaining six P -wave contact terms. But it should be said that this information is not sufficient to pin them down reliably. Note that we set the LEC corresponding to the 1P_1 - 3P_1 transition to zero.

Besides of contact terms with LECs that need to be determined in a fit to data the potential includes also contributions from one-meson and two-meson exchanges. The latter do not involve any free parameters. The coupling constant $f \equiv g_A/2f_0$ is fixed by utilizing the values $g_A = 1.26$ and $f_0 \approx f_\pi = 93$ MeV. For the $F/(F + D)$ -ratio we adopt the SU(6) value $\alpha = 0.4$. It is close to the empirical value of $\alpha \approx 0.36 - 0.37$, as determined recently in analyses

Table 4: The YN contact terms for the P -waves for various cut-offs. The values of the LECs are in 10^4 GeV^{-4} ; the values of Λ in MeV.

Λ		450	500	550	600	650	700
3P_0	$C_{^3P_0}^{27}$	1.47	1.49	1.51	1.55	1.60	1.71
	$C_{^3P_0}^{8_s}$	2.50	2.50	2.50	2.50	2.50	2.50
3P_1	$C_{^3P_1}^{27}$	-0.43	-0.43	-0.43	-0.43	-0.43	-0.43
	$C_{^3P_1}^{8_s}$	0.65	0.65	0.65	0.65	0.65	0.65
3P_2	$C_{^3P_2}^{27}$	-0.096	-0.063	-0.041	-0.025	-0.012	0.000
	$C_{^3P_2}^{8_s}$	1.00	1.00	1.00	1.00	1.00	1.00
1P_1	$C_{^1P_1}^{10}$	0.49	0.49	0.49	0.49	0.49	0.49
	$C_{^1P_1}^{10^*}$	-0.14	-0.14	-0.14	-0.14	-0.14	-0.14
	$C_{^1P_1}^{8_a}$	-0.65	-0.60	-0.58	-0.56	-0.54	-0.52
1P_1 - 3P_1	$C_{^1P_1-^3P_1}^{8_s 8_a}$	0	0	0	0	0	0

of hyperon semi-leptonic decay data [67, 68].

In the spirit of the imposed SU(3) symmetry we keep all contributions from one- and two-meson exchanges, i.e. also those from $\pi\eta$, ηK , KK exchange. The large mass splitting between the Goldstone bosons induces a sizable SU(3) breaking in the actual YN potential that is taken into account in our calculation. There is also an explicit SU(3) symmetry breaking in the coupling constants as reflected in the empirical values of the decay constants f_π , f_K and f_η [69] which, in principle, should be taken into account in the NLO calculation. However, we have ignored such effects in the results reported in the present paper. As a matter of fact, we have explored various scenarios in the course of our investigation. In particular, we performed fits based on the empirical decay constants. We explored also the situation when only $\pi\pi$ exchange diagrams are kept and all two-meson exchanges involving the heavier K , η mesons are omitted. Furthermore, in Ref. [70] we had presented results based on an incomplete NLO calculation, i.e. where only the NLO contact terms were taken into account but no two-meson-exchange contributions. In all these cases a comparable description of the YN data could be achieved, i.e. with a χ^2 within 10-15% of the best values achieved. Seemingly, all two-meson exchange effects could be absorbed into the LECs and, moreover, one could still maintain SU(3) symmetry for these contact terms. A further uncertainty in our calculation is the value of the η -baryon coupling, since we identified the physical η with the octet η_8 . In our earlier investigation [20] we varied the η coupling between zero and its octet value and we found very little influence on the description of the data. Thus, we refrain from introducing a singlet coupling in the present study. It is possible though that future calculations of hypernuclei based on these chiral EFT interactions could indicate a preference for one or the other scenarios and/or yield evidence for the need of an explicit SU(3) breaking in the contact terms.

Finally, let us mention that we did consider also the S -waves for NN scattering. In particular, we fixed the pertinent five LECs from a fit to the np 1S_0 and 3S_1 - 3D_1 phase shifts and mixing parameter in the energy range $T_{lab} \leq 50$ MeV, independently of the YN interaction. Thereby it turned out that the LECs determined from the NN phase shifts are incompatible with those needed for the description of the YN data with regard to the SU(3) symmetry. The most obvious case is the 1S_0 partial wave, where SU(3) symmetry implies that $V_{NN} \equiv V_{\Sigma N}$ ($I=3/2$), see Tab. 1, so that the (hadronic part of the) interaction in the Σ^-n and Σ^+p channels is unambiguously fixed once the LECs are determined from the np phases. However, with LECs determined from the latter channel a near-threshold bound state is obtained in the Σ^+p system and, as a consequence, the empirical $\Sigma^+p \rightarrow \Sigma^+p$ cross section is grossly overestimated. This happens despite of the SU(3) breaking in the interaction that arises from the contributions due to one-meson and two-meson exchanges and despite of the additional Coulomb repulsion in the Σ^+p system. Therefore, we must conclude that within the scheme followed here a combined quantitative description of the NN and YN sectors based on strictly SU(3) symmetric (LO and NLO) contact terms is not possible. Since at NLO an explicit SU(3) breaking in the LO contact terms arises anyway, see Appendix B, we considered also a scenario where we took over the NLO contact terms from the fit to the NN phase shifts and we fitted the remaining (LO and NLO) S -wave contact terms to the YN data. In this case a description of the ΛN and ΣN data is possible, but with a noticeably increased χ^2 . Moreover, we

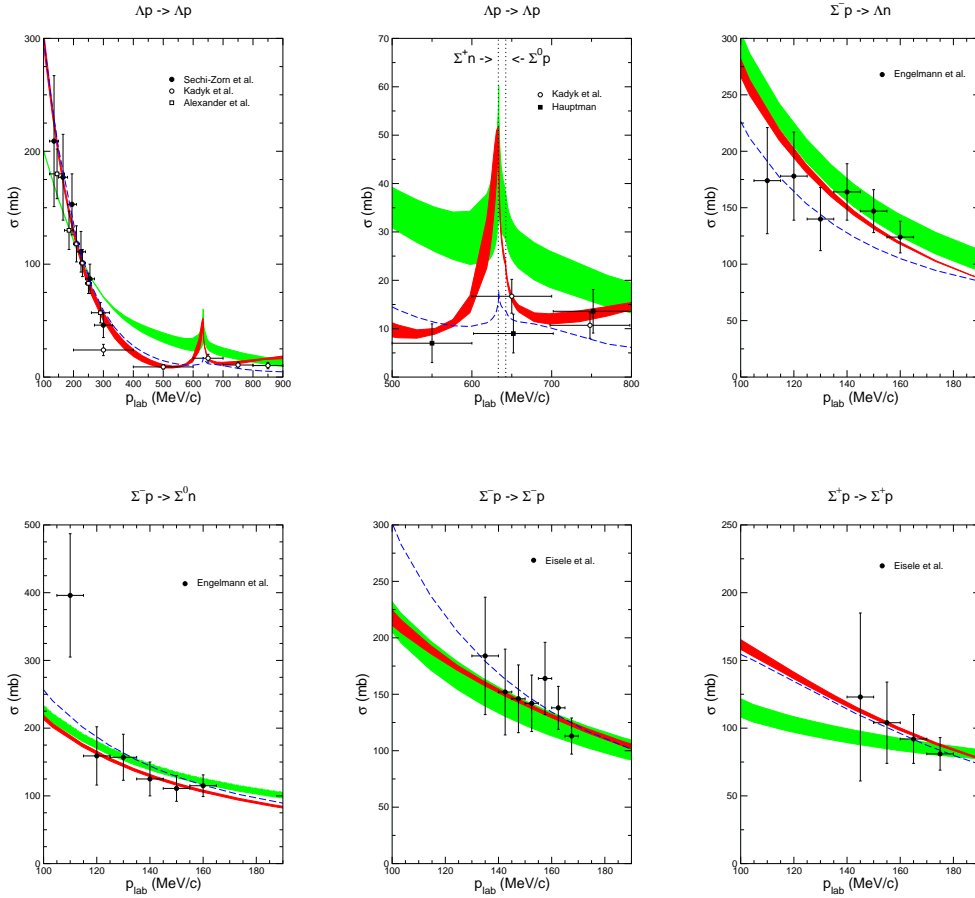


Figure 2: "Total" cross section σ (as defined in Eq. (24)) as a function of p_{lab} . The experimental cross sections are taken from Refs. [52] (filled circles), [53] (open squares), [65] (open circles), and [66] (filled squares) ($\Lambda p \rightarrow \Lambda p$), from [54] ($\Sigma^- p \rightarrow \Lambda n$, $\Sigma^- p \rightarrow \Sigma^0 n$) and from [55] ($\Sigma^- p \rightarrow \Sigma^- p$, $\Sigma^+ p \rightarrow \Sigma^+ p$). The red/dark band shows the chiral EFT results to NLO for variations of the cutoff in the range $\Lambda = 500, \dots, 650$ MeV, while the green/light band are results to LO for $\Lambda = 550, \dots, 700$ MeV. The dashed curve is the result of the Jülich '04 meson-exchange potential [36].

observe the questionable tendency of the Λp amplitude in the 3S_1 partial wave to become rather large for momenta above the ΣN threshold. Thus, we decided to determine all contact terms in the S -waves and the S - D transition from a fit to the YN sector alone where it turns out that $SU(3)$ symmetry for the LECs can be preserved.

The values of the contact terms obtained in the fitting procedure for the various cutoffs are listed in Tables 3 and 4.

4. Results and discussion

The results obtained at NLO are presented in Fig. 2 (red/dark bands), together with those at LO (green/light bands). The bands represent the variation of the cross sections based on chiral EFT within the cutoff region of $\Lambda = 500 - 650$ MeV. Note that in the LO case variations of $\Lambda = 550 - 700$ MeV were considered [20]. For comparison also results for the Jülich '04 [36] meson-exchange model are shown (dashed lines),

Obviously, and as expected, the energy dependence exhibited by the data can be significantly better reproduced within our NLO calculation. This concerns in particular the $\Sigma^+ p$ channel. But also for Λp the NLO results are now

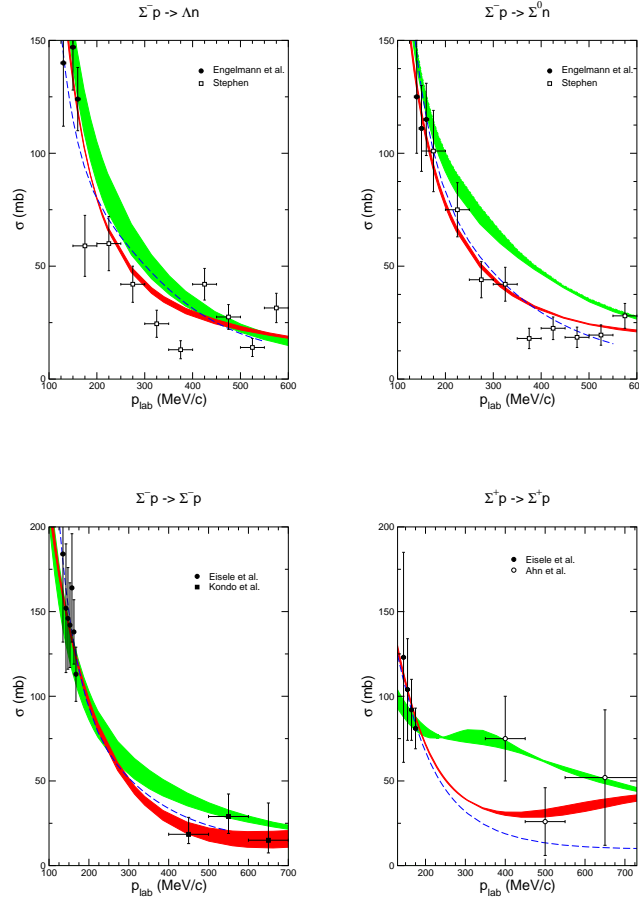


Figure 3: As in Fig. 2, but now the experimental cross sections are taken from Refs. [57] ($\Sigma^- p \rightarrow \Lambda n$, $\Sigma^- p \rightarrow \Sigma^0 n$), [73] ($\Sigma^- p \rightarrow \Sigma^- p$), and [74] ($\Sigma^+ p \rightarrow \Sigma^+ p$).

well in line with the data even up to the ΣN threshold. Furthermore, one can see that the dependence on the cutoff mass is strongly reduced in the NLO case.

A quantitative comparison with the experiments is provided in Tab. 5. There we list the obtained overall χ^2 but also separate values for each data set that was included in the fitting procedure. Obviously the best results are achieved in the range $\Lambda = 500 - 650$ MeV. Here, in addition, the χ^2 exhibits also a fairly weak cutoff dependence so that one can really speak of a plateau region. For larger cutoff values the χ^2 increases smoothly while it grows dramatically when going to lower values. Therefore, in Fig. 2 and in the figures below we show only results based on variations of the cutoff within this plateau region.

A total χ^2 value of around 16 is quite good. Indeed, the best values achieved with phenomenological models, say the Nijmegen NSC97 meson-exchange potentials [37], lie also in that region. We should add that our additional requirements that we want to produce a correctly bound hypertriton and that we want a repulsive ΣN interaction in the isospin $I = 3/2$ channel leads to a slightly increased χ^2 . Without those constraints we could achieve values which are around 5 % smaller. In any case, one has to say that one should not overrate the χ^2 . Given that there are only 36 data points the χ^2 per data point amounts to ≈ 0.5 only – which is somewhat low as compared to what one would expect from a set of statistically sound data. As a matter of fact, the biggest single contribution to the χ^2 comes from the ΣN charge-exchange reaction, see Tab. 5, and specifically from a single data point near threshold that is far off all

Table 5: Comparison between the 36 YN data and the theoretical results for the various cutoffs in terms of the achieved χ^2 . The last column in the NLO section, denoted 600*, contains result for an interaction where all two-meson-exchange contributions involving the η - and/or K meson have been omitted, cf. text.

	data	NLO							LO
Λ (MeV)		450	500	550	600	650	700	600*	600
$\Lambda p \rightarrow \Lambda p$	Sechi-Zorn [52]	2.8	2.1	2.0	1.5	1.6	1.7	1.6	7.5
	Alexander [53]	4.2	2.6	1.6	2.3	2.4	2.5	2.2	4.9
$\Sigma^- p \rightarrow \Lambda n$	Engelmann [54]	4.3	3.7	3.9	4.1	4.4	4.5	4.0	5.5
$\Sigma^- p \rightarrow \Sigma^0 n$	Engelmann [54]	5.6	6.1	5.8	5.8	5.7	5.7	5.9	7.0
$\Sigma^- p \rightarrow \Sigma^- p$	Eisele [55]	2.0	2.0	1.8	1.9	1.9	2.0	1.9	2.4
$\Sigma^+ p \rightarrow \Sigma^+ p$	Eisele [55]	0.5	0.3	0.4	0.5	0.3	0.6	0.9	0.6
r_R	[56, 57]	0.3	0.1	0.2	0.1	0.2	0.3	0.1	0.5
total χ^2		19.7	16.8	15.7	16.2	16.6	17.3	16.5	28.3

other data points, see Fig. 2. When one omits this data point the total χ^2 would be around 10 and the χ^2 per data point would be ≈ 0.3 . Improvements in the order of 5 % on that level are certainly not significant. In this context let us mention the χ^2 of preliminary results of our study that have been presented in [71, 72] is not yet optimal. Specifically, there the description of the $\Sigma^+ p$ cross section was still inferior.

In Table 5 we include also results of an YN interaction where from all two-meson exchange contributions that arise to NLO according to SU(3) symmetry only the $\pi\pi$ exchange diagrams were kept. All two-meson exchange diagrams involving the heavy mesons η and/or K were omitted. We performed an exemplary fit within this scenario for the cutoff $\Lambda = 600$ MeV and the corresponding χ^2 values can be found in the column labeled by 600*. It is obvious that a comparable fit to the data can be achieved within such a scenario, too. Finally, in the last column of Table 5, χ^2 results for our LO interaction from Ref. [20] (for $\Lambda = 600$ MeV) are reproduced. Evidently, going to NLO allows to reduce the χ^2 by roughly 50 %!

A comparison of our results with integrated cross sections at higher energies is presented in Fig. 3. These data were not included in the fitting procedure and, therefore, the shown results are genuine predictions of the chiral EFT interaction. One can see that the cross sections achieved at NLO are now closer to those obtained from the Jülich meson-exchange potential than the ones at LO, and to some extent they are also more in line with the data. But given the large uncertainties in the experiments, even in the fairly recent measurements of the $\Sigma^- p \rightarrow \Sigma^- p$ [73] and $\Sigma^+ p \rightarrow \Sigma^+ p$ [74] reactions, precise conclusions are difficult to draw.

Differential cross sections are shown in Figs. 4 and 5 and compared with available measurements [54, 55, 73, 74, 75]. Also these data were not included in the fitting procedure (as far as the LECs in the S -waves are concerned). However, as already mentioned in the preceding section, the differential cross sections for $\Sigma^- p \rightarrow \Lambda n$ were considered, together with the integrated Λp cross section around $p_{\text{lab}} \approx 750 - 850$ MeV/c, in the “by hand” adjustment of the LECs in the P -waves.

As can be seen from Fig. 4, the prediction of the NLO interaction for $\Sigma^- p \rightarrow \Lambda n$ at $p_{\text{lab}} = 135$ MeV/c agrees well with the trend of the data [54]. The amplitude is dominated by the ${}^3S_1 \rightarrow {}^3S_1$ and ${}^3D_1 \rightarrow {}^3S_1$ transitions so that the resulting angular distribution is rather flat. At LO there are significant P -wave transitions (see the phase shifts discussed below) that give rise to an enhancement of the cross section at backward angles. Such large P -waves arise at LO solely from the one-pion exchange; there are no contact terms yet in those partial waves that would allow one to reduce the P -wave amplitudes as it was possible in the present NLO approach. The resulting cross section at $p_{\text{lab}} = 160$ MeV/c is very similar. Here the data seem to indicate a clear enhancement in forward direction. It should be said, however, that the experimental values shown in Fig. 4 are not the result of a measurement at the specified momenta, but rather an average over different momentum intervals. Specifically, for $\Sigma^- p \rightarrow \Lambda n$ the data [54] are averages over the intervals $100 \leq p_{\Sigma^-} \leq 170$ MeV/c and $150 \leq p_{\Sigma^-} \leq 170$ MeV/c, respectively. In view of the large error bars we refrain here from averaging our theoretical results and, following common practice, present predictions at the average value of the momenta. The same is also true for the data from Ref. [55] which represent averages over

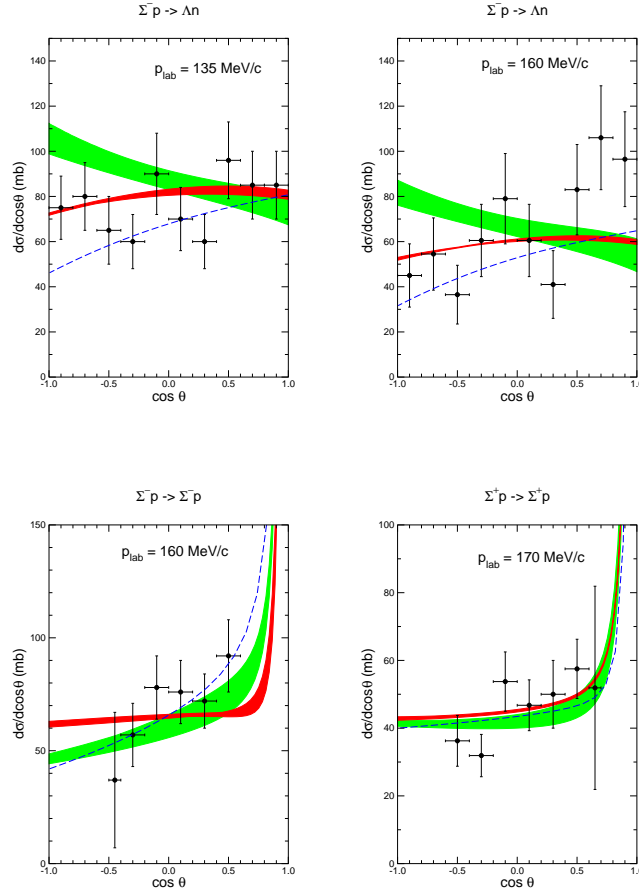


Figure 4: Differential cross section $d\sigma/d\cos\theta$ as a function of $\cos\theta$, where θ is the c.m. scattering angle, at various values of p_{lab} . The experimental differential cross sections are taken from [54] ($\Sigma^-p \rightarrow \Lambda n$, $\Sigma^-p \rightarrow \Sigma^0 n$) and from [55] ($\Sigma^-p \rightarrow \Sigma^- p$, $\Sigma^+p \rightarrow \Sigma^+ p$). Same description of curves as in Fig. 2.

$150 \leq p_{\Sigma^-} \leq 170$ MeV/c (for $\Sigma^-p \rightarrow \Sigma^-p$) and $160 \leq p_{\Sigma^+} \leq 180$ MeV/c (for $\Sigma^+p \rightarrow \Sigma^+p$), respectively.

Fig. 4 suggests that a somewhat different cocktail of P -wave contributions, like the one predicted by the Jülich '04 interaction (cf. the dashed lines), might be more in line with the experimental data. However, we postpone a thorough determination of the LECs in the P -waves to future investigations. Here, as a first step, one would try to connect our interaction with the effective YN interactions in a nuclear medium as determined from the analysis of γ -ray data for Λ hypernuclei [76] via a G -matrix calculation [77]. The results of such an analysis could provide additional and valuable information on the spin-dependence of the YN force and, specifically, on the spin-spin and spin-orbit interaction. Indeed, the spin-orbit splitting of the Λ single-particle levels in nuclei is experimentally well established and very small [78, 79] and, therefore, should constitute a stringent constraint on the interaction. We expect that then also the LEC for the 1P_1 - 3P_1 transition potential can be fixed, which has been set to zero in the present work.

The data on differential cross sections at higher energies (cf. Fig. 5) are averages over $400 \leq p_{\Sigma^-} \leq 700$ MeV/c, for $\Sigma^-p \rightarrow \Sigma^-p$ and over $300 \leq p_{\Sigma^+} \leq 600$ MeV/c [75] and $350 \leq p_{\Sigma^+} \leq 750$ MeV/c [74], respectively, for $\Sigma^+p \rightarrow \Sigma^+p$. Also here the predictions of the YN interactions are for the momenta as specified in Fig. 5.

Scattering lengths for the Λp and Σ^+p interactions in the 1S_0 and 3S_1 partial waves are summarized in Tab. 6. Furthermore we provide results for the hypertriton binding energy. As already said, this binding energy had to be

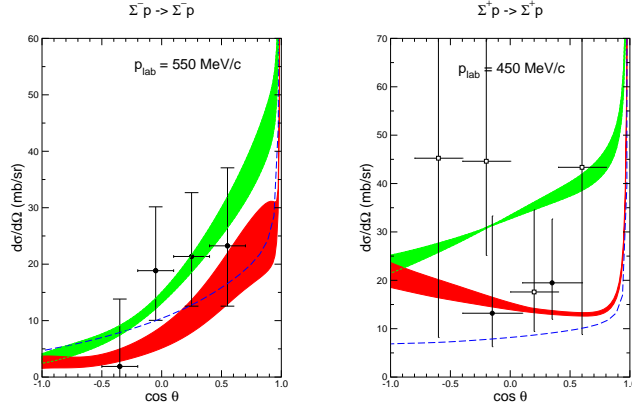


Figure 5: Differential cross section $d\sigma/d\cos\theta$ as a function of $\cos\theta$, where θ is the c.m. scattering angle, at various values of p_{lab} . The experimental differential cross sections are taken from [73] ($\Sigma^- p \rightarrow \Sigma^- p$), and from [75] (filled circles) and [74] (open circles) ($\Sigma^+ p \rightarrow \Sigma^+ p$). Same description of curves as in Fig. 2.

taken as additional constraint in the fitting procedure because otherwise it would have not been possible to fix the relative strength of the (S -wave) singlet- and triplet contributions to the Λp interaction. Tab. 6 lists also results for two meson-exchange potentials, namely of the Jülich '04 model [36] and the Nijmegen NSC97f potential [37], which both reproduce the hypertriton binding energy correctly.

The $\Sigma^+ p$ scattering length in the 3S_1 partial wave is positive, as it was already the case for our LO potential, indicating a repulsive interaction in this channel.

Table 6: The YN singlet (s) and triplet (t) scattering lengths (in fm) and the hypertriton binding energy, E_B (in MeV). The binding energies for the hypertriton (last row) are calculated using the Idaho-N3LO NN potential [27]. The experimental value for the ${}^3_\Lambda\text{H}$ binding energy is $-2.354(50)$ MeV.

	NLO						LO	Jülich '04	NSC97f
	450	500	550	600	650	700	[20]	[36]	[37]
Λ [MeV]							600		
$a_s^{\Lambda p}$	-2.90	-2.91	-2.91	-2.91	-2.90	-2.90	-1.91	-2.56	-2.60
$r_s^{\Lambda p}$	2.64	2.86	2.84	2.78	2.65	2.56	1.40	2.74	3.05
$a_t^{\Lambda p}$	-1.70	-1.61	-1.52	-1.54	-1.51	-1.48	-1.23	-1.67	-1.72
$r_t^{\Lambda p}$	3.44	3.05	2.83	2.72	2.64	2.62	2.13	2.93	3.32
$a_s^{\Sigma^+ p}$	-3.58	-3.59	-3.60	-3.56	-3.46	-3.49	-2.32	-3.60	-4.35
$r_s^{\Sigma^+ p}$	3.49	3.59	3.56	3.54	3.53	3.45	3.60	3.24	3.16
$a_t^{\Sigma^+ p}$	0.48	0.49	0.49	0.49	0.48	0.49	0.65	0.31	-0.25
$r_t^{\Sigma^+ p}$	-4.98	-5.18	-5.03	-5.08	-5.41	-5.18	-2.78	-12.2	-28.9
$({}^3_\Lambda\text{H}) E_B$	-2.39	-2.33	-2.30	-2.30	-2.30	-2.32	-2.34	-2.27	-2.30

The Λp scattering lengths predicted at NLO turn out to be significantly larger than those obtained at LO – as example for the latter we included the result for the cutoff $\Lambda = 600$ MeV in Tab. 6. In case of the 1S_0 channel, they are even somewhat larger than the values of the meson-exchange potentials. We want to remind the reader that the

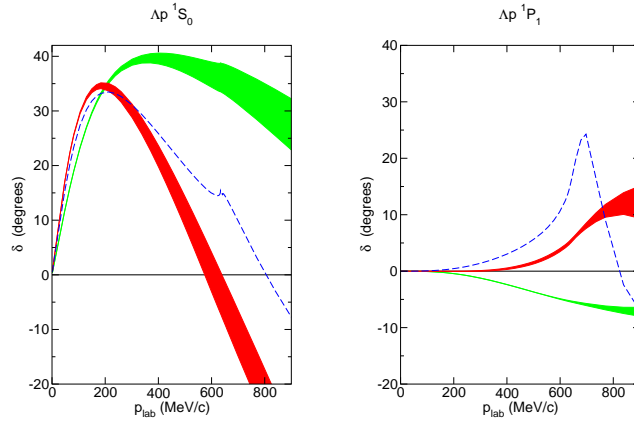


Figure 6: The Λp 1S_0 and 1P_1 phase shifts δ as a function of p_{lab} . The red/dark band shows the chiral EFT results to NLO for variations of the cutoff in the range $\Lambda = 500, \dots, 650$ MeV, while the green/light band are results to LO for $\Lambda = 550, \dots, 700$ MeV. The dashed curve is the result of the Jülich '04 meson-exchange potential [36].

hypertriton binding energy is much more sensitive to the ΛN 1S_0 strength than to that of the 3S_1 - 3D_1 partial wave, as is known from studies in the past [80, 81]. Thus, the value of the 1S_0 scattering length is strongly influenced by our demand to reproduce a correctly bound hypertriton. Interestingly, in the incomplete NLO calculation (i.e. without two-meson-exchange contributions) presented in Ref. [70] a bound hypertriton was achieved with Λp 1S_0 scattering lengths around -2.6 fm, i.e. close to the values of the two meson-exchange potentials, cf. Tab. 6.

The hypertriton results discussed above were all obtained without an explicit three-body force (3BF). It has been argued that the variation of the three-baryon binding energy with the cutoff Λ could provide a measure for the size of the 3BF [82]. If so one would expect its effect to be somewhere in the range of 10-90 keV, based on the values listed in Tab. 6. Formally the first non-vanishing contributions to the 3BF appear at next-to-next-to-leading order (NNLO) in the scheme that we follow [29]. But we want to point out that our present calculation includes already some 3BF effects. These are generated automatically in the employed coupled-channel ΛN - ΣN formalism and occur in the form of the transition of the Λ to the Σ in the intermediate (YNN) state. However, these contributions are two-body reducible and, therefore, do not constitute a genuine (irreducible) 3BF. Note that discussions of 3BF effects in the strangeness sector in the literature [23, 24, 25, 26] are often related to the case of an intermediate Σ , sometimes even exclusively. One should distinguish its role from that of an irreducible 3BF which would be generated, for example, by the excitation of the $\Sigma(1385)$ resonance in the intermediate state – analogous to the 3BF that arises in the standard three-nucleon problem due to the $\Delta(1232)$ excitation.

Calculations for the four-body hypernuclei $^4_\Lambda\text{H}$ and $^4_\Lambda\text{He}$ based on the preliminary version of the NLO interaction presented in [71] can be found in Ref. [82]. That interaction reproduces qualitatively the Λ separation energies for $^4_\Lambda\text{H}$ and, in particular, it yields the correct ordering of the 0^+ and 1^+ states. However, a quantitative agreement with the experimental information is not achieved. Corresponding computations for the EFT interactions discussed in the present paper are in progress [83].

Finally, let us present predictions for a selection of Λp and $\Sigma^+ p$ phase shifts, evaluated in the isospin basis. They can be found in Figs. 6 - 9. The behavior of the 1S_0 phase shift in the Λp channel predicted at NLO is similar to the one of the Jülich '04 model and other meson-exchange potentials [37, 38] though may be slightly more repulsive for higher momenta, cf. Fig. 6. The 1P_1 phase shift is also similar to the result of the Jülich model and has opposite sign as compared to the LO result. Note that this partial wave is the only P -wave where we observed a noticeable cutoff dependence of the results and we counterbalanced this via a smooth variation of the LEC $C_{1P_1}^{\delta_a}$, see Tab. 4. In all other P -waves the value of the additional LEC not determined from the NN sector ($C_{\xi}^{\delta_s}$) is fixed independently of the cutoff Λ .

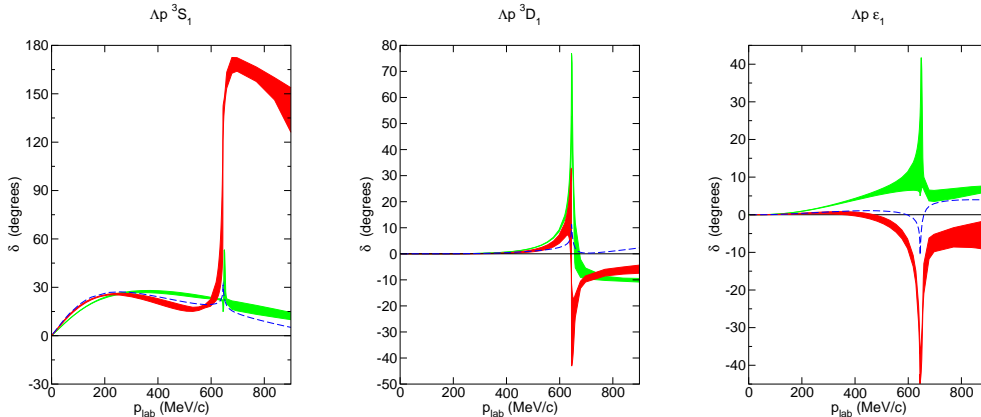


Figure 7: The Λp phase shifts for the coupled 3S_1 - 3D_1 partial wave as a function of p_{lab} . Same description of curves as in Fig. 6.

Phase shifts for the coupled 3S_1 - 3D_1 partial waves and the mixing parameter ϵ_1 can be found in Fig. 7. Evidently, the 3S_1 phase shift based on the NLO interaction passes through 90° slightly below the ΣN threshold. However, also in the 3D_1 phase shift and the mixing parameter we observe an appreciable increase near that threshold. A rise of the 3S_1 (or 3D_1) phase shift beyond 90° is typical for the presence of an unstable bound state in the ΣN system [84, 85], see also the discussion in [86]. In case of the YN interaction at LO and the Jülich '04 model [36] none of the phases pass through 90° and an ordinary cusp is predicted. Such a behavior is caused by an inelastic virtual state in the ΣN system. It should be said, however, that the majority of the meson-exchange potentials [35, 37, 38] produce an unstable bound state, similar to our NLO interaction. The only characteristic difference of the chiral EFT interactions to the meson-exchange potentials might be the mixing parameter ϵ_1 which is fairly large in the former case and close to 45° at the ΣN threshold, see Fig. 7. It is a reflection of the fact that the pertinent Λp T -matrices (for the ${}^3S_1 \rightarrow {}^3S_1$, ${}^3D_1 \rightarrow {}^3D_1$, and ${}^3S_1 \leftrightarrow {}^3D_1$ transitions) are all of the same magnitude. Indeed, these amplitudes yield very similar contributions to the Λp cross section in the vicinity of the ΣN threshold.

In this context let us mention a recent experimental paper where the energy region around the ΣN threshold was investigated in the reaction $pp \rightarrow K^+ \Lambda p$ via a measurement of the Λp invariant mass [87] and where a pronounced structure was observed. For a discussion and summary of older measurements providing evidence for a strong enhancement of the Λp amplitude near the ΣN threshold see Ref. [86].

Predictions for the 3P partial waves of the Λp system are displayed in Fig. 8. One can see that the 3P_0 and 3P_1 phase shifts are reduced at NLO as compared to those obtained at LO while they are larger in case of the 3P_2 . Note that the behavior of the NLO results is strongly influenced by the LECs as fixed from the corresponding NN partial waves because, according to SU(3) symmetry, the pertinent coefficient (C^{27}) dominates also the $\Lambda N \rightarrow \Lambda N$ interaction, see Tab. 1. Obviously, there are sizable quantitative differences between the results for the EFT interaction and the meson-exchange potential.

Results for the $\Sigma^+ p$ system are shown in Fig. 9, where we restrict ourselves to the S -waves. We have switched off the Coulomb interaction for the computation of the phase shifts so that the presented results are those for the ΣN $I = 3/2$ channel. There is no coupling to the ΛN system and therefore the phase shifts are elastic in the momentum region considered.

Both partial waves are quite interesting. First, with regard to the 1S_0 , strict SU(3) symmetry implies that $V_{NN} \equiv V_{\Sigma N}$, see Tab. 1, so that in an exactly SU(3) symmetric world the corresponding pp and $\Sigma^+ p$ phase shifts would be the same. In our calculation we break the symmetry already on the potential level by using the physical masses of the exchanged pseudoscalar mesons and in addition by using the physical baryon masses when solving the LS equation (23). As already mentioned in Sect. 3 we had to introduce also an SU(3) breaking into the contact terms. It turned out to be impossible to describe the pp 1S_0 phase shifts and the $\Sigma^+ p$ cross sections with a consistent set of LECs that

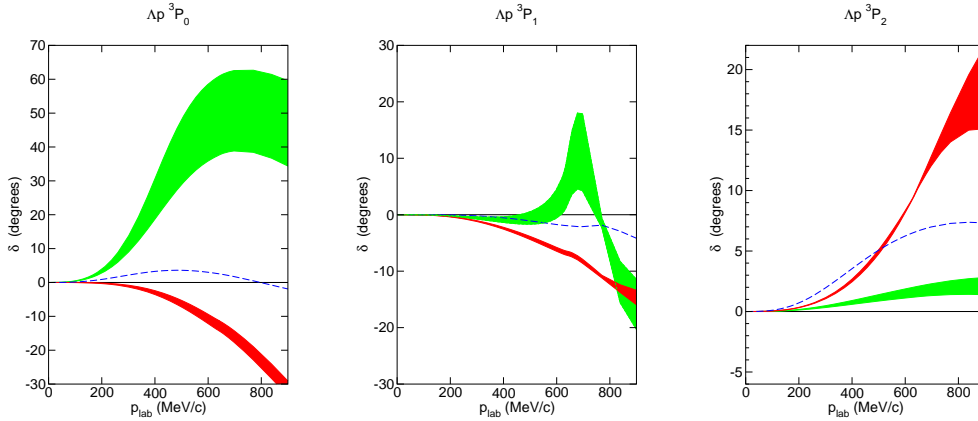


Figure 8: The Λp 3P -wave phase shifts δ as a function of p_{lab} . Same description of curves as in Fig. 6.

fulfill SU(3) symmetry, at least on the level of our NLO calculation. As a matter of fact, the 1S_0 amplitude of our NLO interaction alone saturates already more or less the experimental $\Sigma^+ p$ cross sections. Employing the LECs as fixed from a fit to the pp phase shifts yields a potential that is much more attractive and that produces a near-threshold bound state in the $\Sigma^+ p$ system and, consequently, cross sections that are roughly four times larger than experiment.

Apparently meson-exchange interactions like the Nijmegen potentials are able to describe the NN and YN systems simultaneously, without any major obvious SU(3) breaking. However, usually a special (phenomenological) treatment of the short-ranged part of the potential is required, as discussed, for example, in Ref. [38]. In the potentials of the Jülich group [35, 36] SU(3) symmetry is broken via the employed vertex form factors.

The coupled 3S_1 - 3D_1 partial wave of the $\Sigma^+ p$ system has a strong influence on the properties of the Σ in nuclear matter. Specifically, a repulsive Σ single-particle potential in nuclear matter [62, 63], as supported by present days experimental evidence [59, 60, 61], can only be achieved with a repulsive 3S_1 interaction in the $I = 3/2$ channel. In the course of our investigation we found that we can fit the available YN data equally well with an attractive or a repulsive 3S_1 interaction. The difference in the achieved χ^2 is marginal as already pointed out above. In view of the SU(3) structure given in Tab. 1 this may be not too surprising. The 3S_1 partial wave of the ΣN $I = 3/2$ channel resides in the 10 representation which does not contribute to any of the other NN and YN systems. Of course, its contribution enters indirectly because the measured (physical) reactions $\Sigma^- p \rightarrow \Sigma^- p$ and $\Sigma^- p \rightarrow \Sigma^0 n$ involve amplitudes that result from combinations of the ΣN $I = 3/2$ and $I = 1/2$ interaction potentials.

Our NLO interaction produces a moderately repulsive 3S_1 phase shift as can be seen in Fig. 9, comparable to the one predicted by the LO potential. For the latter, calculations of the Σ single-particle potential have been performed [88] and indicate a values of $U_{\Sigma}(k=0) \approx 12$ MeV at nuclear matter saturation density.

Recent lattice QCD calculations [19] suggest a much more strongly repulsive 3S_1 phase shift in the ΣN $I = 3/2$ channel, when extrapolating the lattice results obtained for $m_{\pi} \approx 389$ MeV to the physical pion mass. But within our framework we cannot accommodate a much more repulsive 3S_1 amplitude. Any sizable increase in the repulsion would yield a 3S_1 amplitude which practically saturates the experimental $\Sigma^+ p$ cross section alone and, consequently, there would be no room anymore for the contribution from the spin-singlet amplitude – which is likewise large as discussed above. Thus, a more strongly repulsive 3S_1 phase shift would immediately result in a dramatic deterioration of the achieved χ^2 .

5. Summary and outlook

Chiral effective field theory, successfully applied in Refs. [27, 28] to the NN interaction, also works well for the baryon-baryon interactions in the strangeness $S = -1$ ($\Lambda N - \Sigma N$) and $S = -2$ ($\Lambda\Lambda - \Xi N - \Sigma\Sigma$) [20, 49] sectors.

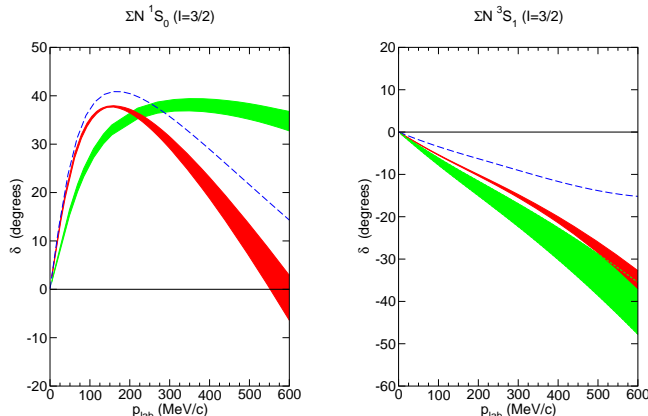


Figure 9: The $\Sigma^+ p$ S -wave phase shifts δ as a function of p_{lab} . Same description of curves as in Fig. 6.

As shown in our earlier work [20], already at leading order the bulk properties of the ΛN and ΣN systems can be reasonably well accounted for. The new results for the YN interaction presented here, obtained to next-to-leading order in the Weinberg counting, are very encouraging. First there is a visible improvement in the quantitative reproduction of the available data on ΛN and ΣN scattering and, secondly, the dependence on the regularization scheme is strongly reduced as compared to the leading-order result. Indeed the description of the YN system achieved at NLO is now on the same level of quality as the one by the most advanced meson-exchange YN interactions.

At the considered order there are contributions from one- and two-pseudoscalar-meson exchange diagrams and from four-baryon contact terms without and with two derivatives. $SU(3)$ flavor symmetry is used as guiding principle in the derivation of the interaction. This means that all the coupling constants at the various baryon-baryon-meson vertices are fixed from $SU(3)$ symmetry and the symmetry is also exploited to derive relations between the contact terms. Furthermore, contributions from all mesons of the pseudoscalar octet (π , K , η) are taken into account. The $SU(3)$ symmetry is, however, broken by the masses of the pseudoscalar mesons and the baryons for which we take the known physical values.

Given the presently available data base with its still large uncertainties, we are able to achieve a combined description of the ΛN and ΣN systems without any explicit $SU(3)$ breaking in the contact interactions. However, we found that a simultaneous description of the NN interaction with contact terms fulfilling strict $SU(3)$ symmetry is not possible. Here the strength of the contact interaction in the 27-representation that is needed to reproduce the pp (or np) 1S_0 phase shifts is simply not compatible with what is required for the description of the empirical $\Sigma^+ p$ cross section.

In any case, it is likely that future (and more precise) data will demand to depart from $SU(3)$ symmetry in the contact terms even with regard to the ΛN and ΣN interactions. Especially studies of few- and many-body systems involving hyperons, which can be done in a consistent way in the framework followed in the present work, could provide evidence for the need of an explicit $SU(3)$ breaking. So far reliable microscopic calculations that utilize directly the elementary YN interaction are only possible (and have been done) for systems with at most four baryons, namely within the Faddeev-Yakubovsky approach [89]. However, it is expected that new approaches that have been developed and refined over the past few years and that are successfully applied in studies of ordinary nuclei allow one to study also hypernuclei with a larger number of baryons with comparable accuracy. Thus, we consider the present investigation as a first and exploratory step towards a more thorough understanding of the baryon-baryon interaction in the strangeness sector.

Acknowledgements

We thank Evgeny Epelbaum for his collaboration in the early stages of this investigation. This work is supported in part by the DFG and the NSFC through funds provided to the Sino-German CRC 110 ‘‘Symmetries and the Emergence of Structure in QCD’’ and by the EU Integrated Infrastructure Initiative HadronPhysics3. S. Petschauer thanks the ‘‘TUM Graduate School’’. Part of the numerical calculations have been performed on the supercomputer cluster of the JSC, Jülich, Germany.

Appendix A. Two-pseudoscalar-meson exchange contributions

In this section we present the next-to-leading order contributions from two-pseudoscalar-meson exchange shown in Fig. 1. The calculation of these potentials was done according to the rules of SU(3) heavy-baryon chiral perturbation theory in the center-of-mass frame and in the isospin limit. Ultraviolet divergences are treated by dimensional regularization, which introduces a scale λ . These divergences are parametrized in an R -term which is absorbed by contact terms. In the used renormalization scheme it is defined as

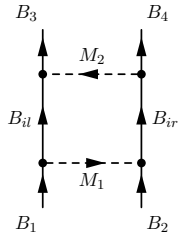
$$R = \frac{2}{d-4} + \gamma_E - 1 - \ln(4\pi), \quad (\text{A.1})$$

with the space-time dimension d .

As for the one-pseudoscalar-meson exchange, Eq. (22), the two-pseudoscalar-meson exchange potentials are given by a general expression, where the proper meson masses have to be inserted, and which has to be multiplied with appropriate SU(3) factors N . We display this factor next to the Feynman diagram and in the corresponding tables. The factors contain coupling constants and isospin factors and are different for each combination of baryons and mesons.

In the following we will show the results for the five diagram types one after another.

Appendix A.1. Planar box



$$N = f_{B_1 B_{4i} M_1} f_{B_{4i} B_3 M_2} f_{B_2 B_{4i} M_1} f_{B_{4i} B_4 M_2} \mathcal{I}_{B_1 B_2 \rightarrow B_3 B_4}$$

Figure A.1: Planar box

The planar box, Fig. A.1, has an irreducible part and a reducible part coming from iterating the one-meson exchange to second order. The reducible part is generated by solving the Lippmann-Schwinger equation and, therefore, is not part of the potential. The irreducible part of this diagram can be obtained by regarding the residues of poles of the meson propagators, but leaving out poles of the baryon propagators. One obtains a central potential ($\mathbb{1}V_C$), a spin-spin potential ($\boldsymbol{\sigma}_1 \cdot \boldsymbol{\sigma}_2 V_S$) and a tensor-type potential ($\boldsymbol{\sigma}_1 \cdot \mathbf{q} \boldsymbol{\sigma}_2 \cdot \mathbf{q} V_T$). With the momentum transfer $q = |\mathbf{p}' - \mathbf{p}|$ and the masses of the two exchanged mesons, m_1 and m_2 , the irreducible potentials can be written in closed analytical form,

$$\begin{aligned} V_{\text{irr,C}}^{\text{planar box}}(q) = & \frac{N}{192\pi^2} \left[\frac{5}{3} q^2 + \frac{(m_1^2 - m_2^2)^2}{q^2} + 16(m_1^2 + m_2^2) + (23q^2 + 45(m_1^2 + m_2^2)) \left(R + 2 \ln \frac{\sqrt{m_1 m_2}}{\lambda} \right) \right. \\ & + \frac{m_1^2 - m_2^2}{q^4} \left(12q^4 + (m_1^2 - m_2^2)^2 - 9q^2(m_1^2 + m_2^2) \right) \ln \frac{m_1}{m_2} + \frac{2}{w^2(q)} \left(23q^4 - \frac{(m_1^2 - m_2^2)^4}{q^4} \right. \\ & \left. \left. + 56(m_1^2 + m_2^2)q^2 + 8 \frac{m_1^2 + m_2^2}{q^2} (m_1^2 - m_2^2)^2 + 2(21m_1^4 + 22m_1^2 m_2^2 + 21m_2^4) \right) L(q) \right], \quad (\text{A.2}) \end{aligned}$$

Table A.1: Isospin factors \mathcal{I} for planar box diagrams. $B_{il}B_{ir}$ indicates the two baryons in the intermediate state and $\pi\pi$ etc. the exchanged pair of mesons M_1M_2 , cf. Fig. A.1.

transition (isospin)	M_1M_2	$\pi\pi$	$\pi\eta$	$\eta\pi$	$\eta\eta$	πK	ηK	M_1M_2	$\bar{K}\pi$	$\bar{K}\eta$	$\bar{K}\bar{K}$
	$B_{il}B_{ir}$							$B_{il}B_{ir}$			
$NN \rightarrow NN$ ($I = 0$)	NN	9	-3	-3	1	0	0	NN	0	0	0
	NN	1	1	1	1	0	0	NN	0	0	0
$\Sigma N \rightarrow \Sigma N$ ($I = 1/2$)	ΣN	4	-2	-2	1	2	-1	$N\Sigma$	2	-1	1
	ΛN	3	0	0	0	3	0	$N\Lambda$	3	0	3
$\Sigma N \rightarrow \Sigma N$ ($I = 3/2$)	ΣN	1	1	1	1	2	2	$N\Sigma$	2	2	4
$\Lambda N \rightarrow \Sigma N$ ($I = 1/2$)	ΣN	$2\sqrt{3}$	$-\sqrt{3}$	0	0	$\sqrt{3}$	0	$N\Sigma$	$2\sqrt{3}$	$-\sqrt{3}$	$\sqrt{3}$
	ΛN	0	0	$-\sqrt{3}$	0	0	$-\sqrt{3}$	$N\Lambda$	$-\sqrt{3}$	0	$-\sqrt{3}$
$\Lambda N \rightarrow \Lambda N$ ($I = 1/2$)	ΣN	3	0	0	0	3	0	$N\Sigma$	3	0	3
	ΛN	0	0	0	1	0	1	$N\Lambda$	0	1	1

$$V_{\text{irr},T}^{\text{planar box}}(q) = -\frac{N}{8\pi^2} \left[L(q) - \frac{1}{2} - \frac{m_1^2 - m_2^2}{2q^2} \ln \frac{m_1}{m_2} + \frac{R}{2} + \ln \frac{\sqrt{m_1 m_2}}{\lambda} \right] = -\frac{1}{q^2} V_{\text{irr},S}^{\text{planar box}}(q), \quad (\text{A.3})$$

where we have defined the functions

$$w(q) = \frac{1}{q} \sqrt{(q^2 + (m_1 + m_2)^2)(q^2 + (m_1 - m_2)^2)}, \quad L(q) = \frac{w(q)}{2q} \ln \frac{(qw(q) + q^2)^2 - (m_1^2 - m_2^2)^2}{4m_1 m_2 q^2}. \quad (\text{A.4})$$

The relation $(\boldsymbol{\sigma}_1 \times \mathbf{q}) \cdot (\boldsymbol{\sigma}_2 \times \mathbf{q}) = \mathbf{q}^2 \boldsymbol{\sigma}_1 \cdot \boldsymbol{\sigma}_2 - (\boldsymbol{\sigma}_1 \cdot \mathbf{q})(\boldsymbol{\sigma}_2 \cdot \mathbf{q})$ is exploited for the connection between the spin-spin and tensor-type potential. The isospin factors \mathcal{I} can be found in Tab. A.1. Two-meson exchange contributions that involve a single K (or \bar{K}) lead to an interchange of the nucleon and the hyperon in the final state. The recoupling of the corresponding isospin states yields a factor (-1) for some of the transitions that is already included in the values given in Tab. A.1. The same applies to the Tables given below. In this context let us mention that for diagrams with an interchange of the nucleon and the hyperon in the final state, likewise an appropriate treatment of the spin-space part is required. In particular, the momentum transfer is then given by $q = |\mathbf{p}' + \mathbf{p}|$.

Note that the potential given above and also the following potentials are finite for $q \rightarrow 0$. Terms proportional to $1/q^2$ and/or $1/q^4$ in Eqs. (A.2) and (A.3) are cancelled by corresponding terms in the functions $L(q)$ and $w(q)$ of Eq. (A.4) in the limit of small q . We perform an expansion of the potentials in a power series for small q so that these cancellations can be taken into account analytically and we obtain stable results in the numerical calculations. For equal meson masses some terms in the potentials vanish and the expressions reduce to the results in Refs. [32, 90]. This is the case in the NN interactions of Refs. [32, 27, 28] based on chiral EFT, where only contributions from two-pion exchange are taken into account.

In the actual calculations only the non-polynomial part of Eqs. (A.2) and (A.3) is taken into account, i.e. the pieces proportional to $L(q)$ and to $1/q^2$ and $1/q^4$. The polynomial part only renormalizes the LO and NLO contact terms and, therefore, is not considered. The contributions involving the regularization scheme (i.e. that depend on R) are likewise omitted. As already said, their effect is assumed to be also absorbed by the contact terms and a renormalization of the coupling constants, see, e.g., the corresponding discussion in Appendix A of [32] for the NN case. We want to remark

that the majority of those terms omitted involve the masses of the pseudoscalar mesons and, therefore, generate an SU(3) symmetry breaking. Thus, the SU(3) symmetry imposed on our contact interaction (at least for ΛN and ΣN) is understood as one that is fulfilled on the level of the renormalized coupling constants.

All statements above apply also to the other contributions to the potential described below.

Appendix A.2. Crossed box

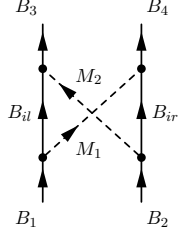


Figure A.2: Crossed box

$$N = f_{B_1 B_i} M_1 f_{B_i B_3} M_2 f_{B_2 B_i} M_2 f_{B_i B_4} M_1 \mathcal{I}_{B_1 B_2 \rightarrow B_3 B_4}$$

The crossed box diagrams, Fig. A.2, yield a central, a spin-spin, and a tensor-type potential. Due to the similar structure but different kinematics, the potentials resulting from the crossed boxes are the same as those of the planar box, up to a sign:

$$V_C^{\text{crossed box}}(q) = -V_{C, \text{irr}}^{\text{planar box}}(q), \quad (\text{A.5})$$

$$V_T^{\text{crossed box}}(q) = -\frac{1}{q^2} V_S^{\text{crossed box}}(q) = V_{T, \text{irr}}^{\text{planar box}}(q). \quad (\text{A.6})$$

Note that there is no iterated part in case of the crossed boxes. The corresponding isospin factors \mathcal{I} can be found in Tab. A.2.

Appendix A.3. Triangles

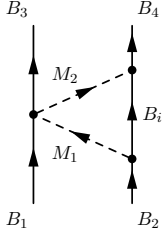


Figure A.3: Left triangle

$$N = f_{B_2 B_i} M_1 f_{B_i B_4} M_2 \mathcal{I}_{B_1 B_2 \rightarrow B_3 B_4}$$

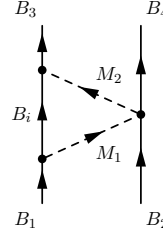


Figure A.4: Right triangle

$$N = f_{B_1 B_i} M_1 f_{B_i B_3} M_2 \mathcal{I}_{B_1 B_2 \rightarrow B_3 B_4}$$

The two triangle diagrams, Figs. A.3 and A.4, lead to equal potentials, but with different SU(3) factors. They contribute only to the central potential and the corresponding expression is given by

$$V_C^{\text{triangle}}(q) = -\frac{N}{768\pi^2 f_0^2} \left[-2(m_1^2 + m_2^2) + \frac{(m_1^2 - m_2^2)^2}{q^2} - \frac{13}{3}q^2 + \left(8(m_1^2 + m_2^2) - \frac{2(m_1^2 - m_2^2)^2}{q^2} + 10q^2 \right) L(q) \right. \\ \left. + \frac{m_1^2 - m_2^2}{q^4} \left((m_1^2 - m_2^2)^2 - 3(m_1^2 + m_2^2)q^2 \right) \ln \frac{m_1}{m_2} + (9(m_1^2 + m_2^2) + 5q^2) \left(R + 2 \ln \frac{\sqrt{m_1 m_2}}{\lambda} \right) \right]. \quad (\text{A.7})$$

The isospin factors \mathcal{I} are stated in Tables A.3 and A.4.

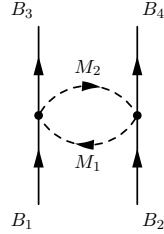
Table A.2: Isospin factors I for crossed box diagrams. $B_{il}B_{ir}$ indicates the two baryons in the intermediate state and $\pi\pi$ etc. the exchanged pair of mesons M_1M_2 , cf. Fig. A.2.

transition (isospin)	M_1M_2	$\pi\pi$	$\pi\eta$	$\eta\pi$	$\eta\eta$	$\bar{K}\pi$	$\bar{K}\eta$	M_1M_2	πK	ηK	KK
	$B_{il}B_{ir}$							$B_{il}B_{ir}$			
$NN \rightarrow NN$ ($I = 0$)	NN	-3	-3	-3	1	0	0	$\Sigma\Sigma$	0	0	3
								$\Lambda\Sigma, \Sigma\Lambda$	0	0	3
$(I = 1)$	NN	5	1	1	1	0	0	$\Lambda\Lambda$	0	0	-1
								$\Sigma\Sigma$	0	0	5
								$\Lambda\Sigma, \Sigma\Lambda$	0	0	1
								$\Lambda\Lambda$	0	0	1
$\Sigma N \rightarrow \Sigma N$ ($I = 1/2$)	ΣN	0	-2	-2	1	0	0	$\Sigma\Sigma$	0	-1	0
	NN	0	0	0	0	5	-1	$\Xi\Sigma$	0	0	5
$(I = 3/2)$	ΛN	-1	0	0	0	0	0	$\Lambda\Lambda$	1	0	0
								$\Xi\Lambda$	0	0	-1
								$\Lambda\Sigma, \Sigma\Lambda$	2	0	0
	ΣN	3	1	1	1	0	0	$\Sigma\Sigma$	3	2	0
	NN	0	0	0	0	2	2	$\Xi\Sigma$	0	0	2
	ΛN	2	0	0	0	0	0	$\Lambda\Lambda$	1	0	0
								$\Xi\Lambda$	0	0	2
								$\Lambda\Sigma, \Sigma\Lambda$	-1	0	0
$\Lambda N \rightarrow \Sigma N$ ($I = 1/2$)	ΣN	$-2\sqrt{3}$	$-\sqrt{3}$	0	0	0	0	$\Sigma\Sigma$	$2\sqrt{3}$	0	0
	NN	0	0	0	0	$\sqrt{3}$	$-\sqrt{3}$	$\Xi\Sigma$	0	0	$-\sqrt{3}$
	ΛN	0	0	$-\sqrt{3}$	0	0	0	$\Sigma\Lambda$	$-\sqrt{3}$	0	0
								$\Lambda\Sigma$	0	$-\sqrt{3}$	0
								$\Xi\Lambda$	0	0	$\sqrt{3}$
$\Lambda N \rightarrow \Lambda N$ ($I = 1/2$)	ΣN	3	0	0	0	0	0	$\Sigma\Sigma$	3	0	0
	NN	0	0	0	0	3	1	$\Xi\Sigma$	0	0	3
	ΛN	0	0	0	1	0	0	$\Xi\Lambda$	0	0	1
								$\Lambda\Lambda$	0	1	0

Table A.3: Isospin factors \mathcal{I} for triangle diagrams with the $BBMM$ vertex at the left baryon. B_i denotes the baryon in the intermediate state and $\pi\pi$ etc. the exchanged pair of mesons M_1M_2 , cf. Fig. A.3.

transition (isospin)	$\begin{array}{c} \backslash M_1 M_2 \\ B_i \end{array}$	$\pi\pi$	$\pi\bar{K}$	$\eta\bar{K}$	$\bar{K}\bar{K}$	$\begin{array}{c} \backslash M_1 M_2 \\ B_i \end{array}$	$K\pi$	$K\eta$	KK
$NN \rightarrow NN$									
$(I = 0)$	N	12	0	0	0	Σ	0	0	-12
$(I = 1)$	N	-4	0	0	0	Σ	0	0	-8
						Λ	0	0	-4
$\Sigma N \rightarrow \Sigma N$									
$(I = 1/2)$	N	16	1	$-\sqrt{3}$	0	Σ	-2	$\sqrt{3}$	-4
		0	0	0	0	Λ	1	0	4
$(I = 3/2)$	N	-8	-2	$2\sqrt{3}$	0	Σ	4	$-2\sqrt{3}$	2
		0	0	0	0	Λ	-2	0	-2
$\Lambda N \rightarrow \Sigma N$									
$(I = 1/2)$	N	0	3	$-3\sqrt{3}$	0	Σ	-6	$3\sqrt{3}$	0
		0	0	0	0	Λ	3	0	0
$\Lambda N \rightarrow \Lambda N$									
$(I = 1/2)$	N	0	$3\sqrt{3}$	3	0	Σ	$-3\sqrt{3}$	0	0
		0	0	0	0	Λ	0	-3	0

Appendix A.4. Football



$$N = \mathcal{I}_{B_1 B_2 \rightarrow B_3 B_4}$$

Figure A.5: Football diagram

The football diagrams, Fig. A.5, give contributions to the central potential only,

$$\begin{aligned}
 V_C^{\text{football}}(q) = & \frac{N}{3072\pi^2 f_0^4} \left[-2(m_1^2 + m_2^2) - \frac{(m_1^2 - m_2^2)^2}{2q^2} - \frac{5}{6}q^2 + (3(m_1^2 + m_2^2) + q^2) \left(\frac{R}{2} + \ln \frac{\sqrt{m_1 m_2}}{\lambda} \right) \right. \\
 & \left. - \frac{m_1^2 - m_2^2}{2q^4} \left((m_1^2 - m_2^2)^2 + 3(m_1^2 + m_2^2)q^2 \right) \ln \frac{m_1}{m_2} + w^2(q) L(q) \right]. \quad (\text{A.8})
 \end{aligned}$$

The isospin factors \mathcal{I} can be found in Table A.5.

Table A.4: Isospin factors \mathcal{I} for triangle diagrams with the $BBMM$ vertex at the right baryon. B_i denotes the baryon in the intermediate state and $\pi\pi$ etc. the exchanged pair of mesons M_1M_2 , cf. Fig. A.4.

transition (isospin)	M_1M_2 B_i	$\pi\pi$	πK	ηK	KK	M_1M_2 B_i	$\bar{K}\pi$	$\bar{K}\eta$	$\bar{K}\bar{K}$	
$NN \rightarrow NN$ ($I = 0$)	N	12	0	0	0					
	Σ	0	0	0	-12					
	(I = 1)	N	-4	0	0	0				
		Σ	0	0	0	-8				
		Λ	0	0	0	-4				
$\Sigma N \rightarrow \Sigma N$ ($I = 1/2$)	Σ	4	-2	$\sqrt{3}$	0	N	1	$-\sqrt{3}$	10	
	Λ	4	1	0	0					
	(I = 3/2)	Ξ	0	0	0	-2				
		Σ	-2	4	$-2\sqrt{3}$	0	N	-2	$2\sqrt{3}$	4
		Λ	-2	-2	0	0				
Ξ	0	0	0	-8						
$\Lambda N \rightarrow \Sigma N$ ($I = 1/2$)	Σ	$4\sqrt{3}$	$3\sqrt{3}$	0	0	N	$-3\sqrt{3}$	-3	$-2\sqrt{3}$	
	Λ	0	0	3	0					
	Ξ	0	0	0	$-2\sqrt{3}$					
$\Lambda N \rightarrow \Lambda N$ ($I = 1/2$)	Λ	0	0	-3	0	N	$3\sqrt{3}$	3	6	
	Σ	0	$-3\sqrt{3}$	0	0					
	Ξ	0	0	0	-6					

Table A.5: Isospin factors \mathcal{I} for football diagrams. $\pi\pi$ etc. indicates the exchanged pair of mesons M_1M_2 , cf. Fig. A.5.

transition (isospin)	$\pi\pi$	$K\pi$	$K\eta$	$\pi\bar{K}$	$\eta\bar{K}$	KK	$\bar{K}\bar{K}$
$NN \rightarrow NN$							
($I = 0$)	-24	0	0	0	0	12	12
($I = 1$)	8	0	0	0	0	20	20
$\Sigma N \rightarrow \Sigma N$							
($I = 1/2$)	-32	-3	-3	-3	-3	-8	-8
($I = 3/2$)	16	6	6	6	6	4	4
$\Lambda N \rightarrow \Sigma N$							
($I = 1/2$)	0	-9	-9	-9	-9	0	0
$\Lambda N \rightarrow \Lambda N$							
($I = 1/2$)	0	9	9	9	9	0	0

Appendix B. SU(3) breaking

Appendix B.1. SU(3) breaking in the contact terms

In addition to the SU(3) symmetric contact terms given in Sect. 2 that arise at NLO, there are further contact terms at this order that lead to an explicit SU(3) symmetry breaking. These terms contain new, i.e. additional, low-energy constants. As already mentioned in Sect. 3, the lack of experimental data makes it practically impossible to fix those contact terms and, therefore, we decided to set all the corresponding constants to zero. However, for completeness and for future reference, we summarize here the structure of the pertinent contributions.

First there would be, in principle, relativistic corrections ($1/M_B$) to the leading order contact terms [20],

$$\mathcal{L}_1 = C_1^i \text{tr} \left((\bar{B}^\alpha (\Gamma^i B)_\alpha \bar{B}^\beta (\Gamma^i B)_\beta) \right), \quad \mathcal{L}_2 = C_2^i \text{tr} \left(\bar{B}^\alpha \bar{B}^\beta (\Gamma^i B)_\beta (\Gamma^i B)_\alpha \right), \quad \mathcal{L}_3 = C_3^i \text{tr} \left(\bar{B}^\alpha (\Gamma^i B)_\alpha \right) \text{tr} \left(\bar{B}^\beta (\Gamma^i B)_\beta \right), \quad (\text{B.1})$$

which break SU(3) symmetry because of different baryon masses. Here a sum over the different elements of the Dirac algebra, $\Gamma^i \in \{\mathbb{1}, \gamma_\mu, \gamma_5, \gamma_5 \gamma_\mu, \sigma_{\mu\nu}\}$, is implied. The indices α and β are Dirac indices. However, since the corrections to the baryon mass in the chiral limit are of order $\mathcal{O}(q^2)$, explicit symmetry breaking due to these corrections does not appear up to NLO.

However, NLO contact terms with an insertion of the external field χ , which is of order $\mathcal{O}(q^2)$, are possible. In the case of baryon-baryon scattering that field amounts to

$$\chi = 2B_0 \begin{pmatrix} m_u & 0 & 0 \\ 0 & m_d & 0 \\ 0 & 0 & m_s \end{pmatrix} \approx \begin{pmatrix} m_\pi^2 & 0 & 0 \\ 0 & m_\pi^2 & 0 \\ 0 & 0 & 2m_K^2 - m_\pi^2 \end{pmatrix}. \quad (\text{B.2})$$

The following baryon-baryon contact terms with insertions of χ are possible [48]:

$$\begin{aligned} \mathcal{L}_1 &= C_1^i \text{tr} \left(\bar{B}^\alpha \chi (\Gamma^i B)_\alpha \bar{B}^\beta (\Gamma^i B)_\beta \right), \\ \mathcal{L}_2 &= C_2^i \text{tr} \left(\bar{B}^\alpha (\Gamma^i B)_\alpha \chi \bar{B}^\beta (\Gamma^i B)_\beta \right), \\ \mathcal{L}_3 &= C_3^i \text{tr} \left(\bar{B}^\alpha \chi \bar{B}^\beta (\Gamma^i B)_\beta (\Gamma^i B)_\alpha \right) + \text{tr} \left(\bar{B}^\alpha \bar{B}^\beta (\Gamma^i B)_\beta \chi (\Gamma^i B)_\alpha \right), \end{aligned}$$

$$\begin{aligned}
\mathcal{L}_4 &= C_4^i \text{tr} \left(\bar{B}^\alpha \bar{B}^\beta \chi (\Gamma^i B)_\beta (\Gamma^i B)_\alpha \right), \\
\mathcal{L}_5 &= C_5^i \text{tr} \left(\bar{B}^\alpha \bar{B}^\beta (\Gamma^i B)_\beta (\Gamma^i B)_\alpha \chi \right), \\
\mathcal{L}_6 &= C_6^i \text{tr} \left(\bar{B}^\alpha (\Gamma^i B)_\alpha \chi \right) \text{tr} \left(\bar{B}^\beta (\Gamma^i B)_\beta \right), \\
\mathcal{L}_7 &= C_7^i \text{tr} \left(\bar{B}^\alpha \chi \right) \text{tr} \left((\Gamma^i B)_\alpha \bar{B}^\beta (\Gamma^i B)_\beta \right) + \text{tr} \left(\bar{B}^\alpha (\Gamma^i B)_\alpha \bar{B}^\beta \right) \text{tr} \left((\Gamma^i B)_\beta \chi \right),
\end{aligned} \tag{B.3}$$

and lead to an explicit SU(3) symmetry breaking linear in the quark masses, since we use $m_u = m_d \neq m_s$. Using these Lagrangians one obtains terms that contribute to the 1S_0 and 3S_1 partial waves (only). In the following we list the results for different transitions (with isospin I).

$NN \rightarrow NN$, $I = 0$:

$$V(^1S_0) = 0, \tag{B.4}$$

$$\begin{aligned}
V(^3S_1) &= 4\pi \left[4C_{^3S_1}^1 m_\pi^2 + C_{^3S_1}^2 (8m_K^2 - 4m_\pi^2) + C_{^3S_1}^6 (8m_K^2 - 4m_\pi^2) \right] \\
&= m_\pi^2 \hat{C}^{10^*},
\end{aligned} \tag{B.5}$$

$NN \rightarrow NN$, $I = 1$:

$$\begin{aligned}
V(^1S_0) &= 4\pi \left[4C_{^1S_0}^1 m_\pi^2 + C_{^1S_0}^2 (8m_K^2 - 4m_\pi^2) + C_{^1S_0}^6 (8m_K^2 - 4m_\pi^2) \right] \\
&= m_\pi^2 \hat{C}^{27},
\end{aligned} \tag{B.6}$$

$$V(^3S_1) = 0, \tag{B.7}$$

$\Lambda N \rightarrow \Lambda N$, $I = 1/2$:

$$\begin{aligned}
V(^1S_0) &= 4\pi \left[\frac{1}{3} C_{^1S_0}^1 (4m_K^2 + m_\pi^2) + C_{^1S_0}^2 \left(3m_K^2 - \frac{4}{3} m_\pi^2 \right) + C_{^1S_0}^3 \left(\frac{4}{3} m_K^2 - m_\pi^2 \right) + \frac{1}{6} C_{^1S_0}^4 m_\pi^2 \right. \\
&\quad \left. + \frac{1}{6} C_{^1S_0}^5 (2m_K^2 - m_\pi^2) + \frac{2}{3} C_{^1S_0}^6 (5m_K^2 - 2m_\pi^2) + \frac{4}{3} C_{^1S_0}^7 (m_K^2 - m_\pi^2) \right] \\
&= \frac{1}{10} m_\pi^2 (9\hat{C}^{27} + \hat{C}^{8s}),
\end{aligned} \tag{B.8}$$

$$\begin{aligned}
V(^3S_1) &= 4\pi \left[\frac{1}{3} C_{^3S_1}^1 (4m_K^2 - m_\pi^2) + \frac{1}{3} C_{^3S_1}^2 (7m_K^2 - 4m_\pi^2) + C_{^3S_1}^3 (4m_K^2 - m_\pi^2) + \frac{3}{2} C_{^3S_1}^4 m_\pi^2 \right. \\
&\quad \left. + C_{^3S_1}^5 \left(3m_K^2 - \frac{3}{2} m_\pi^2 \right) + \frac{2}{3} C_{^3S_1}^6 (5m_K^2 - 2m_\pi^2) + 4C_{^3S_1}^7 (m_K^2 - m_\pi^2) \right] \\
&= \frac{1}{2} m_\pi^2 (\hat{C}^{10^*} + \hat{C}^{8a}),
\end{aligned} \tag{B.9}$$

$\Lambda N \rightarrow \Sigma N$, $I = 1/2$:

$$\begin{aligned}
V(^1S_0) &= 4\pi \left[C_{^1S_0}^1 m_\pi^2 + C_{^1S_0}^2 m_K^2 + C_{^1S_0}^3 (m_\pi^2 - 2m_K^2) - \frac{1}{2} C_{^1S_0}^4 m_\pi^2 + \frac{1}{2} C_{^1S_0}^5 (m_\pi^2 - 2m_K^2) - 2C_{^1S_0}^7 (m_\pi^2 + m_K^2) \right] \\
&= \frac{3}{10} m_\pi^2 (\hat{C}^{8s} - \hat{C}^{27}) + (m_K^2 - m_\pi^2) \hat{C}_1,
\end{aligned} \tag{B.10}$$

$$\begin{aligned}
V(^3S_1) &= 4\pi \left[-C_{^3S_1}^1 m_\pi^2 - C_{^3S_1}^2 m_K^2 + C_{^3S_1}^3 (2m_K^2 + m_\pi^2) + \frac{3}{2} C_{^3S_1}^4 m_\pi^2 + C_{^3S_1}^5 (3m_K^2 - \frac{3}{2} m_\pi^2) + 2C_{^3S_1}^7 (m_K^2 - m_\pi^2) \right] \\
&= \frac{1}{2} m_\pi^2 (\hat{C}^{10^*} - \hat{C}^{8a}) + (m_K^2 - m_\pi^2) \hat{C}_2,
\end{aligned} \tag{B.11}$$

$\Sigma N \rightarrow \Sigma N$, $I = 1/2$:

$$\begin{aligned}
V(^1S_0) &= 4\pi \left[-C_{^1S_0}^1 m_\pi^2 - C_{^1S_0}^2 m_K^2 + 3C_{^1S_0}^3 m_\pi^2 + \frac{3}{2} C_{^1S_0}^4 m_\pi^2 + \frac{3}{2} C_{^1S_0}^5 (2m_K^2 - m_\pi^2) + 2C_{^1S_0}^6 m_K^2 \right] \\
&= \frac{1}{10} m_\pi^2 (\hat{C}^{27} + 9\hat{C}^{8s}) + (m_K^2 - m_\pi^2) \hat{C}_3,
\end{aligned} \tag{B.12}$$

$$\begin{aligned}
V(^3S_1) &= 4\pi \left[C_{^3S_1}^1 m_\pi^2 + C_{^3S_1}^2 m_K^2 + 3C_{^3S_1}^3 m_\pi^2 + \frac{3}{2} C_{^3S_1}^4 m_\pi^2 + \frac{3}{2} C_{^3S_1}^5 (2m_K^2 - m_\pi^2) + 2C_{^3S_1}^6 m_K^2 \right] \\
&= \frac{1}{2} m_\pi^2 (\hat{C}^{10^*} + \hat{C}^{8a}) + (m_K^2 - m_\pi^2) \hat{C}_4,
\end{aligned} \tag{B.13}$$

$\Sigma N \rightarrow \Sigma N$, $I = 3/2$:

$$\begin{aligned} V(^1S_0) &= 4\pi \left[2C_{1S_0}^1 m_\pi^2 + 2C_{1S_0}^2 m_K^2 + 2C_{1S_0}^6 m_K^2 \right] \\ &= m_\pi^2 \hat{C}^{27} + (m_K^2 - m_\pi^2) \hat{C}_5, \end{aligned} \quad (\text{B.14})$$

$$\begin{aligned} V(^3S_1) &= 4\pi \left[-2C_{3S_1}^1 m_\pi^2 - 2C_{3S_1}^2 m_K^2 + 2C_{3S_1}^6 m_K^2 \right] \\ &= m_\pi^2 \hat{C}^{10}. \end{aligned} \quad (\text{B.15})$$

We introduced here appropriately redefined constants \hat{C} so that the SU(3) breaking is clearly visible. In case of flavor symmetry where $m_\pi = m_K$ the leading order SU(3) relations, cf. Tab. 1, are obtained and the constants can be absorbed in the leading order contact terms. If $m_\pi \neq m_K$ one obtains additional (though suppressed) constants that are proportional to $m_K^2 - m_\pi^2$.

Appendix B.2. SU(3) breaking in the OBE contribution

At NLO and NNLO there are corrections to the one-meson exchange potential due to differences in the baryon masses. Energy conservation leads to

$$\sqrt{\mathbf{p}^2 + M_{B_1}^2} + \sqrt{\mathbf{p}^2 + M_{B_2}^2} = \sqrt{\mathbf{p}'^2 + M_{B_3}^2} + \sqrt{\mathbf{p}'^2 + M_{B_4}^2}, \quad (\text{B.16})$$

and, therefore, in some cases $\mathbf{p}^2 \neq \mathbf{p}'^2$ and/or $q_0 \neq 0$, where

$$q^0 = \Delta E = E_{p'}^3 - E_p^1 = E_p^2 - E_{p'}^4. \quad (\text{B.17})$$

Using $M_{B_i} = M_0 + O(p^2)$ [50] and performing an expansion in $1/M_0$ one obtains

$$\begin{aligned} V_{B_1 B_2 \rightarrow B_3 B_4}^{OBE} &= -f_{B_1 B_3 P} f_{B_2 B_4 P} \bar{J}_{B_1 B_2 \rightarrow B_3 B_4} \frac{1}{\mathbf{q}^2 - q_0^2 + m_P^2} \left[\boldsymbol{\sigma}_1 \cdot \mathbf{q} \boldsymbol{\sigma}_2 \cdot \mathbf{q} \right. \\ &\quad \left. + \frac{\mathbf{p}'^2 - \mathbf{p}^2}{4M_0^2} (\boldsymbol{\sigma}_1 \cdot \mathbf{p}' \boldsymbol{\sigma}_2 \cdot \mathbf{p}' - \boldsymbol{\sigma}_1 \cdot \mathbf{p} \boldsymbol{\sigma}_2 \cdot \mathbf{p}) + \frac{q_0}{M_0} (\boldsymbol{\sigma}_1 \cdot \mathbf{p} \boldsymbol{\sigma}_2 \cdot \mathbf{p}' - \boldsymbol{\sigma}_1 \cdot \mathbf{p}' \boldsymbol{\sigma}_2 \cdot \mathbf{p}) \right]. \end{aligned} \quad (\text{B.18})$$

The first term gives rise to the leading order tensor potential, see Eq. (22), but with a shift $\mathbf{q}^2 \rightarrow \mathbf{q}^2 - q_0^2$ caused by the mass differences of the baryons, i.e. $q^0 \approx \Delta M$ where $\Delta M = (M_{B_1} + M_{B_4} - M_{B_3} - M_{B_2})/2$ [38]. The last two terms in Eq. (B.18) give a formal contribution beyond LO. The term proportional to $(\mathbf{p}'^2 - \mathbf{p}^2)$ contributes, in general, only off-shell. An exception are transitions where the baryon masses in the initial state are not equal to those of the final state, cf. Eq. (B.16). For the YN interaction considered here this is only the case for the $V_{\Lambda N \rightarrow \Sigma N}$ transition potential. In the present study we have neglected all these corrections.

There are also deviations of the meson-baryon coupling constants from the SU(3) values which, in principle, should be taken into account in a NLO calculation. Specifically, there is an explicit SU(3) symmetry breaking in the empirical values of the decay constants [69],

$$f_\pi = 92.4 \text{ MeV}, \quad f_\eta = (1.19 \pm 0.01)f_\pi, \quad f_K = (1.30 \pm 0.05)f_\pi. \quad (\text{B.19})$$

A somewhat smaller SU(3) breaking occurs also in the axial coupling constants, see [67, 68, 91] but also [92, 93]. All these effects are likewise not taken into account in the present study. Rather we use the standard SU(3) relations for the baryon-baryon-meson coupling constants Eq. (21) with the values $g_A = 1.26$ and $f_0 \approx f_\pi = 93 \text{ MeV}$.

References

- [1] see list of proposals at http://j-parc.jp/researcher/Hadron/en/Proposal_e.html
- [2] W. Erni *et al.* [Panda Collaboration], arXiv:0903.3905 [hep-ex].

- [3] F. Hiruma *et al.*, http://j-parc.jp/researcher/Hadron/en/pac_1101/pdf/KEK_J-PARC-PAC2010-12.pdf
- [4] M. Röder, PhD thesis, Bochum (2011); M. Röder *et al.*, in preparation.
- [5] K. Hicks *et al.*, *Measurement of the ΛN interaction with a deuterium target*, <http://www.rcnp.osaka-u.ac.jp/Divisions/plan/q-pac/ex-appro/prop/Q026.pdf>
- [6] S. C. Pieper and R. B. Wiringa, *Ann. Rev. Nucl. Part. Sci.* **51** (2001) 53.
- [7] A. Kievsky, S. Rosati, M. Viviani, L. E. Marcucci and L. Girlanda, *J. Phys. G* **35** (2008) 063101.
- [8] P. Navrátil, S. Quaglioni, I. Stetcu and B. R. Barrett, *J. Phys. G* **36** (2009) 083101.
- [9] R. Roth, S. Binder, K. Vobig, A. Calci, J. Langhammer and P. Navratil, *Phys. Rev. Lett.* **109** (2012) 052501 [arXiv:1112.0287 [nucl-th]].
- [10] B. Borasoy, E. Epelbaum, H. Krebs, D. Lee and U.-G. Meißner, *Eur. Phys. J. A* **31** (2007) 105 [nucl-th/0611087].
- [11] D. Lee, *Prog. Part. Nucl. Phys.* **63** (2009) 117.
- [12] G. Hagen, T. Papenbrock, D.J. Dean, A. Schwenk, A. Nogga, M. Wloch and P. Piecuch, *Phys. Rev. C* **76** (2007) 034302.
- [13] G. Hagen, D.J. Dean, M. Hjorth-Jenson, T. Papenbrock and A. Schwenk, *Phys. Rev. C* **76** (2007) 044305.
- [14] E. Epelbaum, H. Krebs, D. Lee and U.-G. Meißner, *Phys. Rev. Lett.* **106** (2011) 192501 [arXiv:1101.2547 [nucl-th]].
- [15] H. Nemura, Y. Akaishi and Y. Suzuki, *Phys. Rev. Lett.* **89** (2002) 142504.
- [16] E. Hiyama, M. Kamimura, Y. Yamamoto, T. Motoba and T. A. Rijken, *Prog. Theor. Phys. Suppl.* **185** (2010) 106.
- [17] S. R. Beane, W. Detmold, K. Orginos and M. J. Savage, *Prog. Part. Nucl. Phys.* **66** (2011) 1.
- [18] S. Aoki *et al.* [HAL QCD Collaboration], *Prog. Theor. Exp. Phys.* **2012** (2012) 01A105.
- [19] S. R. Beane *et al.*, *Phys. Rev. Lett.* **109** (2012) 172001.
- [20] H. Polinder, J. Haidenbauer and U.-G. Meißner, *Nucl. Phys. A* **779** (2006) 244.
- [21] S. Weinberg, *Phys. Lett. B* **251** (1990) 288.
- [22] S. Weinberg, *Nucl. Phys. B* **363** (1991) 3.
- [23] R. K. Bhaduri, B. Loiseau, and Y. Nogami, *Ann. Phys. (N. Y.)* **44** (1967) 57.
- [24] A. Gal, J.M. Soper, and R.H. Dalitz, *Ann. Phys. (N. Y.)* **63** (1971) 53.
- [25] J. Schaffner-Bielich, *Nucl. Phys. A* **835** (2010) 279.
- [26] I. Vidana, D. Logoteta, C. Providencia, A. Polls and I. Bombaci, *Europhys. Lett.* **94** (2011) 11002.
- [27] D. R. Entem, R. Machleidt, *Phys. Rev. C* **68** (2003) 041001.
- [28] E. Epelbaum, W. Glöckle, U.-G. Meißner, *Nucl. Phys. A* **747** (2005) 362.
- [29] E. Epelbaum, H. -W. Hammer and U.-G. Meißner, *Rev. Mod. Phys.* **81** (2009) 1773.
- [30] R. Machleidt and D. R. Entem, *Phys. Rept.* **503** (2011) 1 [arXiv:1105.2919 [nucl-th]].
- [31] E. Epelbaum, W. Glöckle, U.-G. Meißner, *Nucl. Phys. A* **637** (1998) 107.
- [32] E. Epelbaum, W. Glöckle, U.-G. Meißner, *Nucl. Phys. A* **671** (2000) 295.
- [33] C. L. Korpa, A. E. L. Dieperink, R. G. E. Timmermans, *Phys. Rev. C* **65** (2001) 015208.
- [34] S. R. Beane, P. F. Bedaque, A. Parreño, M. J. Savage, *Nucl. Phys. A* **747** (2005) 55.
- [35] B. Holzenkamp, K. Holinde, J. Speth, *Nucl. Phys. A* **500** (1989) 485.
- [36] J. Haidenbauer, U.-G. Meißner, *Phys. Rev. C* **72** (2005) 044005.
- [37] T. A. Rijken, V. G. J. Stoks, Y. Yamamoto, *Phys. Rev. C* **59** (1999) 21.
- [38] T. A. Rijken, M. M. Nagels, Y. Yamamoto, *Prog. Theor. Phys. Suppl.* **185** (2010) 14.
- [39] A. Nogga, R. G. E. Timmermans and U. van Kolck, *Phys. Rev. C* **72** (2005) 054006.
- [40] M. Pavon Valderama, E. Ruiz Arriola, *Phys. Rev. C* **74** (2006) 054001.
- [41] R. Machleidt, Q. MacPherson, E. Marji, R. Winzer, C. Zeoli and D. R. Entem, arXiv:1210.0992 [nucl-th].
- [42] D. R. Phillips, arXiv:1302.5959 [nucl-th].
- [43] J. Haidenbauer, U.-G. Meißner, *Phys. Lett. B* **684** (2010) 275.
- [44] J. Haidenbauer, U.-G. Meißner, A. Nogga and H. Polinder, *Lect. Notes Phys.* **724** (2007) 113.
- [45] S. Petschauer, diploma thesis, TU Munich, 2011.
- [46] J. J. de Swart, *Rev. Mod. Phys.* **35** (1963) 916.
- [47] C. B. Dover and H. Feshbach, *Annals Phys.* **217** (1992) 51.
- [48] S. Petschauer and N. Kaiser, in preparation.
- [49] H. Polinder, J. Haidenbauer and U.-G. Meißner, *Phys. Lett. B* **653** (2007) 29.
- [50] V. Bernard, N. Kaiser, U.-G. Meißner, *Int. J. Mod. Phys. E* **4** (1995) 193.
- [51] C.M. Vincent and S.C. Phatak, *Phys. Rev. C* **10** (1974) 391.
- [52] B. Sechi-Zorn, B. Kehoe, J. Twitty, R. A. Burnstein, *Phys. Rev.* **175** (1968) 1735.
- [53] G. Alexander, U. Karshon, A. Shapira, G. Yekutieli, R. Engelmann, H. Filthuth, W. Lughofer, *Phys. Rev.* **173** (1968) 1452.
- [54] R. Engelmann, H. Filthuth, V. Hepp, E. Kluge, *Phys. Lett.* **21** (1966) 587.
- [55] F. Eisele, H. Filthuth, W. Fölisch, V. Hepp, G. Zech, *Phys. Lett.* **37B** (1971) 204.
- [56] V. Hepp and H. Schleich, *Z. Phys.* **214** (1968) 71.
- [57] D. Stephen, Ph.D. thesis, University of Massachusetts, unpublished (1970).
- [58] J. J. de Swart, C. Dullemond, *Ann. Phys.* **19** (1962) 485.
- [59] S. Bart *et al.*, *Phys. Rev. Lett.* **83** (1999) 5238.
- [60] H. Noumi *et al.*, *Phys. Rev. Lett.* **89** (2002) 072301; **90** (2003) 049902 (E).
- [61] P.K. Saha *et al.*, *Phys. Rev. C* **70** (2004) 044613.
- [62] M. Kohno, Y. Fujiwara, Y. Watanabe, K. Ogata and M. Kawai, *Phys. Rev. C* **74** (2006) 064613.
- [63] J. Dabrowski and J. Rozynek, *Phys. Rev. C* **78** (2008) 037601.
- [64] V. G. J. Stoks, R. A. M. Klomp, C. P. F. Terheggen and J. J. de Swart, *Phys. Rev. C* **49** (1994) 2950.
- [65] J. A. Kadyk, G. Alexander, J. H. Chan, P. Gaposchkin, G. H. Trilling, *Nucl. Phys. B* **27** (1971) 13.
- [66] J. M. Hauptman, J. A. Kadyk, G. H. Trilling, *Nucl. Phys. B* **125** (1977) 29.

- [67] P. G. Ratcliffe, Phys. Lett. B **365** (1996) 383.
- [68] T. Yamanishi, Phys. Rev. D **76** (2007) 014006.
- [69] J. Beringer *et al.* [Particle Data Group], Phys. Rev. D **86** (2012) 010001.
- [70] J. Haidenbauer, EPJ Web of Conferences **3** (2010) 01009.
- [71] J. Haidenbauer, arXiv:1301.1141 [nucl-th], Nucl. Phys. A, in press.
- [72] J. Haidenbauer, in *Proceedings of The 7th International Workshop on Chiral Dynamics*, 6-10 August, 2012, Newport News, USA, in press.
- [73] Y. Kondo *et al.*, Nucl. Phys. A **676** (2000) 371.
- [74] J. K. Ahn *et al.*, Nucl. Phys. A **761** (2005) 41.
- [75] J. K. Ahn *et al.*, Nucl. Phys. A **648** (1999) 263.
- [76] D. J. Millener, Nucl. Phys. A **881** (2012) 298.
- [77] A. Reuber, K. Holinde and J. Speth, Nucl. Phys. A **570** (1994) 543.
- [78] O. Hashimoto and H. Tamura, Prog. Part. Nucl. Phys. **57** (2006) 564.
- [79] N. Kaiser and W. Weise, Phys. Rev. C **71** (2005) 015203
- [80] B. F. Gibson and D. R. Lehman, Phys. Rev. C **22** (1980) 2024.
- [81] K. Miyagawa, H. Kamada, W. Glöckle, V. G. J. Stoks, Phys. Rev. C **51** (1995) 2905.
- [82] A. Nogga, Proceedings of the *XI International Conference on Hypernuclear and Strange Particle Physics*, Barcelona, October 1 - 5, 2012, Nucl. Phys. A, in press.
- [83] A. Nogga, J. Haidenbauer, and U.-G. Meißner, in preparation.
- [84] A. M. Badalyan, L. P. Kok, M. I. Polikarpov, Y. A. Simonov, Phys. Rep. **82** (1982) 31.
- [85] K. Miyagawa, H. Yamamura, Phys. Rev. C **60** (1999) 024003.
- [86] H. Machner, J. Haidenbauer, F. Hinterberger, A. Magiera, J. A. Niskanen, J. Ritman and R. Siudak, Nucl. Phys. A **901** (2013) 65.
- [87] S. A. El-Samad *et al.* [COSY TOF Collaboration], arXiv:1206.0426 [nucl-ex].
- [88] M. Kohno, Phys. Rev. C **81** (2010) 014003.
- [89] A. Nogga, H. Kamada and W. Gloeckle, Phys. Rev. Lett. **88** (2002) 172501.
- [90] N. Kaiser, R. Brockmann, W. Weise, Nucl. Phys. A **625** (1997) 758.
- [91] J. F. Donoghue and B. R. Holstein, Phys. Rev. D **25** (1982) 2015.
- [92] V. Bernard, L. Elouadrhiri and U.-G. Meißner, J. Phys. G **28** (2002) R1.
- [93] I. J. General and S. R. Cotanch, Phys. Rev. C **69** (2004) 035202.